



## WETCHIMP-WSL: intercomparison of wetland methane emissions models over West Siberia

T. J. Bohn<sup>1</sup>, J. R. Melton<sup>2</sup>, A. Ito<sup>3</sup>, T. Kleinen<sup>4</sup>, R. Spahni<sup>5,6</sup>, B. D. Stocker<sup>5,7</sup>, B. Zhang<sup>8</sup>, X. Zhu<sup>9,10,11</sup>, R. Schroeder<sup>12,13</sup>, M. V. Glagolev<sup>14,15,16,17</sup>, S. Maksyutov<sup>3,16</sup>, V. Brovkin<sup>4</sup>, G. Chen<sup>18</sup>, S. N. Denisov<sup>19</sup>, A. V. Eliseev<sup>19,20</sup>, A. Gallego-Sala<sup>21</sup>, K. C. McDonald<sup>12</sup>, M.A. Rawlins<sup>22</sup>, W. J. Riley<sup>11</sup>, Z. M. Subin<sup>11</sup>, H. Tian<sup>8</sup>, Q. Zhuang<sup>9</sup>, and J. O. Kaplan<sup>23</sup>

<sup>1</sup>School of Earth and Space Exploration, Arizona State University, Tempe, AZ, USA

<sup>2</sup>Canadian Centre for Climate Modelling and Analysis, Environment Canada, Victoria, BC, Canada

<sup>3</sup>National Institute for Environmental Studies, Tsukuba, Japan

<sup>4</sup>Max Planck Institute for Meteorology, Hamburg, Germany

<sup>5</sup>Climate and Environmental Physics, Physics Institute, University of Bern, Bern, Switzerland

<sup>6</sup>Oeschger Centre for Climate Change Research, University of Bern, Bern, Switzerland

<sup>7</sup>Department of Life Sciences, Imperial College, Silwood Park Campus, Ascot, UK

<sup>8</sup>International Center for Climate and Global Change Research and School of Forestry and Wildlife Sciences, Auburn University, Auburn, AL, USA

<sup>9</sup>Department of Earth, Atmospheric, and Planetary Sciences, Purdue University, West Lafayette, IN, USA

<sup>10</sup>Natural Resource Ecology Laboratory, Colorado State University, Fort Collins, CO, USA

<sup>11</sup>Earth Sciences Division, Lawrence Berkeley National Laboratory, Berkeley, CA, USA

<sup>12</sup>City College of New York, City University of New York, New York, NY, USA

<sup>13</sup>Institute of Botany, University of Hohenheim, Stuttgart, Germany

<sup>14</sup>Moscow State University, Moscow, Russia

<sup>15</sup>Institute of Forest Science, Russian Academy of Sciences, Uspenskoe, Russia

<sup>16</sup>Laboratory of Computational Geophysics, Tomsk State University, Tomsk, Russia

<sup>17</sup>Yugra State University, Khanty-Mantsiysk, Russia

<sup>18</sup>Oak Ridge National Laboratory, Oak Ridge, TN, USA

<sup>19</sup>A. M. Obukhov Institute of Atmospheric Physics, Russian Academy of Sciences, Moscow, Russia

<sup>20</sup>Kazan Federal University, Kazan, Russia

<sup>21</sup>Department of Geography, University of Exeter, Exeter, UK

<sup>22</sup>Department of Geosciences, University of Massachusetts, Amherst, MA, USA

<sup>23</sup>Institute of Earth Surface Dynamics, University of Lausanne, Lausanne, Switzerland

*Correspondence to:* T. J. Bohn (theodore.bohn@asu.edu)

Received: 10 December 2014 – Published in Biogeosciences Discuss.: 30 January 2015

Revised: 29 April 2015 – Accepted: 30 April 2015 – Published: 3 June 2015

**Abstract.** Wetlands are the world's largest natural source of methane, a powerful greenhouse gas. The strong sensitivity of methane emissions to environmental factors such as soil temperature and moisture has led to concerns about potential positive feedbacks to climate change. This risk is particularly relevant at high latitudes, which have experienced pronounced warming and where thawing permafrost

could potentially liberate large amounts of labile carbon over the next 100 years. However, global models disagree as to the magnitude and spatial distribution of emissions, due to uncertainties in wetland area and emissions per unit area and a scarcity of in situ observations. Recent intensive field campaigns across the West Siberian Lowland (WSL) make this an ideal region over which to assess the per-

formance of large-scale process-based wetland models in a high-latitude environment. Here we present the results of a follow-up to the Wetland and Wetland CH<sub>4</sub> Intercomparison of Models Project (WETCHIMP), focused on the West Siberian Lowland (WETCHIMP-WSL). We assessed 21 models and 5 inversions over this domain in terms of total CH<sub>4</sub> emissions, simulated wetland areas, and CH<sub>4</sub> fluxes per unit wetland area and compared these results to an intensive in situ CH<sub>4</sub> flux data set, several wetland maps, and two satellite surface water products. We found that (a) despite the large scatter of individual estimates, 12-year mean estimates of annual total emissions over the WSL from forward models ( $5.34 \pm 0.54$  Tg CH<sub>4</sub> yr<sup>-1</sup>), inversions ( $6.06 \pm 1.22$  Tg CH<sub>4</sub> yr<sup>-1</sup>), and in situ observations ( $3.91 \pm 1.29$  Tg CH<sub>4</sub> yr<sup>-1</sup>) largely agreed; (b) forward models using surface water products alone to estimate wetland areas suffered from severe biases in CH<sub>4</sub> emissions; (c) the interannual time series of models that lacked either soil thermal physics appropriate to the high latitudes or realistic emissions from unsaturated peatlands tended to be dominated by a single environmental driver (inundation or air temperature), unlike those of inversions and more sophisticated forward models; (d) differences in biogeochemical schemes across models had relatively smaller influence over performance; and (e) multiyear or multidecade observational records are crucial for evaluating models' responses to long-term climate change.

## 1 Introduction

Methane (CH<sub>4</sub>) emissions from high-latitude wetlands are an important component of the global climate system. CH<sub>4</sub> is an important greenhouse gas, with approximately 34 times the global warming potential of carbon dioxide (CO<sub>2</sub>) over a century time horizon (IPCC, 2013). Globally, wetlands are the largest natural source of CH<sub>4</sub> emissions to the atmosphere (IPCC, 2013). Because wetland CH<sub>4</sub> emissions are highly sensitive to soil temperature and moisture conditions (Saarnio et al., 1997; Friborg et al., 2003; Christensen et al., 2003; Moore et al., 2011; Glagolev et al., 2011; Sabrekov et al., 2014), there is concern that they will provide positive feedback to future climate warming (Gedney et al., 2004; Eliseev et al., 2008; Ringeval et al., 2011). This risk is particularly important in the world's high latitudes because they contain nearly half of the world's wetlands (Lehner and Döll, 2004) and because the high latitudes have been and are forecast to continue experiencing more rapid warming than elsewhere (Serreze et al., 2000; IPCC, 2013). Adding to these concerns is the potential liberation (and possible conversion to CH<sub>4</sub>) of previously frozen, labile soil carbon from thawing permafrost over the next century (Christensen et al., 2004; Schuur et al., 2008; Koven et al., 2011; Schaefer et al., 2011).

Process-based models are crucial for increasing our understanding of the response of wetland CH<sub>4</sub> emissions to climate change. Large-scale biogeochemical models, especially those embedded within earth system models, are particularly important for estimating the magnitudes of feedbacks to climate change (e.g., Gedney et al., 2004; Eliseev et al., 2008; Koven et al., 2011). However, as shown in the global Wetland and Wetland CH<sub>4</sub> Intercomparison of Models Project (WETCHIMP; Melton et al., 2013; Wania et al., 2013), there was wide disagreement among large-scale models as to the magnitude of global and regional wetland CH<sub>4</sub> emissions, in terms of both wetland areas and CH<sub>4</sub> emissions per unit wetland area. These discrepancies were due in part to the large variety of schemes used for representing hydrological and biogeochemical processes, in part to uncertainties in model parameterizations, and in part to the sparseness of in situ observations with which to evaluate model performance (Melton et al., 2013).

In addition to these challenges on the global scale, the unique characteristics of high-latitude environments pose further problems for biogeochemical models. For example, much of the northern land surface is underlain by permafrost, which impedes drainage (Smith et al., 2005) and stores ancient carbon (Koven et al., 2011) via temperature-dependent constraints on carbon cycling (Schoor et al., 2008). Similarly, peat soils and winter snowpack can thermally insulate soils (Zhang, 2005; Lawrence and Slater, 2008, 2010), dampening their sensitivities to interannual variability in climate. Several commonly used global biogeochemical models (e.g., Tian et al., 2010; Hopcroft et al., 2011; Hodson et al., 2011; Kleinen et al., 2012) lack representations of some or all of these processes.

The prevalence of peatlands in the high-latitudes poses further challenges to modeling (Frolking et al., 2009). Peatlands are a type of wetland containing deep deposits of highly porous, organic-rich soil, formed over thousands of years under waterlogged and anoxic conditions, which inhibit decomposition (Gorham, 1991; Frolking et al., 2011). Within the porous soil, the water table is often only a few centimeters below the surface, leading to anoxic conditions and CH<sub>4</sub> emissions even when no surface water is present (Saarnio et al., 1997; Friborg et al., 2003; Glagolev et al., 2011). This condition can lead to an underestimation of wetland area when using satellite surface water products as inputs to wetland methane emissions models. In addition, trees and shrubs are found with varying frequency in peatlands (e.g., Shimoyama et al., 2003; Efremova et al., 2014), interfering with the detection of inundation. Furthermore, the water table depth within a peatland is typically heterogeneous, varying on the scale of tens of centimeters as a function of microtopography (hummocks, hollows, ridges, and pools; Eppinga et al., 2008). Models vary widely in their representations of wetland soil moisture conditions, ranging from schemes that do not explicitly consider the water table position (e.g., Hodson et al., 2011) to a single uniform water table depth for

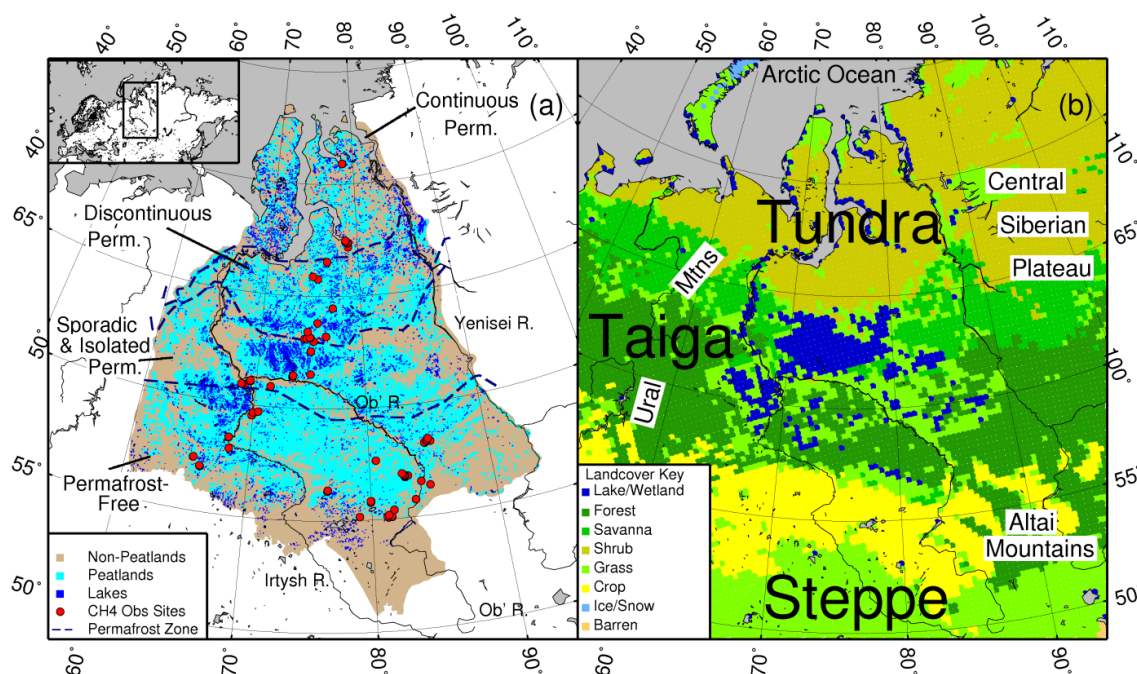


**Figure 1.** Map of the West Siberian Lowland (WSL). (a) Limits of domain (brown) and peatland distribution (cyan), taken from Sheng et al. (2004); lakes of area  $> 1 \text{ km}^2$  (blue) taken from Lehner and Döll (2004); permafrost zone boundaries after Kremenetski et al. (2003);  $\text{CH}_4$  sampling sites from Glagolev et al. (2011), denoted by red circles. (b) Dominant land cover at 25 km derived from MODIS-MOD12Q1 500 m land cover classification (Friedl et al., 2010).

each grid cell (e.g., Zhuang et al., 2004) to more sophisticated schemes that allow for sub-grid heterogeneity in the water table (e.g., Bohn et al., 2007, 2013; Ringeval et al., 2010; Riley et al., 2011; Kleinen et al., 2012; Stocker et al., 2014; Subin et al., 2014). Finally, peatland soils can be highly acidic and nutrient-poor, and much of the available carbon substrate can be recalcitrant (Clymo et al., 1984; Dorrepaal et al., 2009). While some models attempt to account for the effects of soil chemical conditions such as pH, redox potential, and nutrient limitation (e.g., Zhuang et al., 2004; Riley et al., 2011; Sabrekov et al., 2013; Spahni et al., 2013), not all do.

Given the potential problems of parameter uncertainty and equifinality (Tang and Zhuang, 2008; van Huissteden et al., 2009) and computational limitations when wetland components are embedded within global climate models, it is important to determine which model features are necessary to simulate high-latitude peatlands accurately and to constrain parameter values with observations. Until recently, the evaluation of large-scale wetland  $\text{CH}_4$  emissions models has been difficult, due to the sparseness of in situ and atmospheric  $\text{CH}_4$  observations. However, observations from the West Siberian Lowland (WSL) now offer the opportunity to assess model performance, thanks to recent intensive field campaigns (Glagolev et al., 2011), aircraft profiles (Umezawa et al., 2012), tall-tower observations (Sasakawa et al., 2010; Winderlich et al., 2010), and high-resolution wet-

land inventories (Sheng et al., 2004; Peregon et al., 2008, 2009).

Our primary goal in this study is to determine how well current global large-scale models capture the dynamics of high-latitude wetland  $\text{CH}_4$  emissions. To this end, we assess the performance of 21 large-scale wetland  $\text{CH}_4$  emissions models over West Siberia, relative to in situ and remotely sensed observations as well as inverse models. We examine both spatial and temporal accuracy, including seasonal and interannual variability, and estimate the relative influences of environmental drivers on model behaviors. We identify the dominant sources of error and the model features that may have caused them. Finally, we make recommendations as to which model features are necessary for accurate simulations of high-latitude wetland  $\text{CH}_4$  emissions and which types of observations would help improve future efforts to constrain model behaviors.

## 2 Methods

### 2.1 Spatial domain

The West Siberian Lowland (WSL) occupies approximately 2.5 million  $\text{km}^2$  in northern central Eurasia, spanning from 50 to 75° N and 60 to 95° E (Fig. 1a). This region is bounded on the west by the Ural Mountains; on the east by the Yenisei River and the Central Siberian Plateau; on the north by the

Arctic Ocean; and on the south by the Altai Mountains and the grasslands of the Eurasian Steppe (Sheng et al., 2004). The WSL contains most of the drainage areas of the Ob' and Irtysh rivers, as well as the western tributaries of the Yenisei River, all of which drain into the Arctic Ocean. Permafrost in various forms (continuous, discontinuous, isolated, and sporadic) covers more than half of the area of the WSL, from the Arctic Ocean south to approximately 60° N, with continuous permafrost occurring north of 67° N (Kremenetski et al., 2003). The region's major biomes (Fig. 1b) consist of the treeless tundra north of 66° N, approximately coincident with continuous permafrost; the taiga forest belt between 55 and 66° N; and the grasslands of the steppe south of 55° N.

Wetlands occupy 600 000 km<sup>2</sup>, or about 25 % of the land area of the WSL, primarily in the taiga and tundra zones (Sheng et al., 2004). The vast majority of these wetlands are peatlands, which have peat depths ranging from 50 cm to over 5 m and which comprise a total soil carbon pool of 70 Pg C (Sheng et al., 2004). Numerous field studies have documented strong methane emissions from these peatlands, particularly those south of the southern limit of permafrost (e.g., Sabrekov et al., 2014; Sasakawa et al., 2012; Glagolev et al., 2011, 2012; Friborg et al., 2003; Shimoyama et al., 2003; Panikov and Dedysh, 2000). Permanent water bodies, ranging in size from lakes 100 km<sup>2</sup> in area to pools only a few meters across, are comingled with wetlands throughout the domain (Lehner and Döll, 2004; Repo et al., 2007; Eppinga et al., 2008). Notable concentrations of lakes are found (a) north of the Ob' River between 61 and 64° N and 68 and 80° E; (b) west of the confluence of the Ob' and Irtysh rivers between 59 and 61° N and 64 and 70° E; and (c) on the Yamal Peninsula north of 68° N.

Because the vegetative and soil conditions vary substantially across the domain, we have divided it into two halves of approximately equal size along 61° N latitude. The region north of this line contains permafrost, while the region south of the line is essentially permafrost-free.

## 2.2 Terminology

Estimating wetland CH<sub>4</sub> emissions over large scales requires accurately delineating the wetland area over which CH<sub>4</sub> emissions can occur. Unfortunately, "wetland" definitions vary within the scientific community (Mitsch and Gosselink, 2000). For the purposes of estimating CH<sub>4</sub> emissions, the key characteristics include anoxia and available labile carbon substrate; therefore, we will adopt the definition proposed by Canada's National Wetlands Working Group (Tarnocai et al., 1988): land that is saturated with water for long enough to promote wetland or aquatic processes as indicated by poorly drained soils, hydrophytic vegetation, and various kinds of biological activity which are adapted to a wet environment. Because permanent, deep (> 2m) open-water bodies are subject to additional processes (e.g., allochthonous carbon inputs, wind-driven mixing of the water column; Pace et al., 2004),

we will exclude them from our definition. Unfortunately, explicit observations of lake depths are lacking for all but the deepest lakes; therefore, we will instead use an area threshold (1 km<sup>2</sup>) to identify permanent lakes. This definition of wetlands therefore includes all peatlands (inundated or not), seasonally inundated non-peatland soils (e.g., river floodplains), and small ponds or lakes but excludes rivers and large lakes.

We define "surface water" as all freshwater above the soil surface, i.e., the superset of inundation, lakes, and rivers. We define "inundation" as temporary (present for less than 1 year) standing water above the soil surface; "lakes" as permanent water bodies (present for more than 1 year) exceeding 1 km<sup>2</sup> in area; and "rivers" as channels that carry turbulent water. Surface water therefore includes areas that do not emit large amounts of CH<sub>4</sub>, such as rivers, and also excludes some CH<sub>4</sub>-emitting areas such as non-inundated peatlands.

For models, we will use the term "CH<sub>4</sub>-producing area" to refer to the area over which CH<sub>4</sub> production is simulated, which might not coincide exactly with the areas of actual or simulated wetlands.

## 2.3 Observations and inversions

Table 1 lists the various observations and inversions that we used in this study. We considered four wetland map products over the WSL, all of which have been used in high-latitude wetland carbon studies. Two of them are regional maps specific to the WSL: Sheng et al. (2004), denoted by "Sheng2004", and Peregon et al. (2008), denoted by "Peregon2008". Both Sheng 2004 and Peregon2008 used the 1 : 2500 000-scale map of Romanova (1977); Peregon2008 was entirely based on the Romanova map, while Sheng2004 used the Romanova map north of 65° N and used the 1 : 100 000-scale maps of Markov (1971) and Matukhin and Danilov (2000) elsewhere. Both of these maps delineate the extents of peatlands, including ponds and lakes smaller than 1 km<sup>2</sup> in area. The Sheng2004 product additionally includes a separate layer delineating lakes larger than 1 km<sup>2</sup>. The Peregon2008 product distinguishes between various wetland subtypes (e.g., sphagnum- or sedge-dominated bogs and high *palsa mires*). The third map is the Northern Circumpolar Soil Carbon Database (NCSCD; Tarnocai et al., 2009), an inventory of carbon-rich soils, including peatlands, within the Arctic permafrost region. Models that have used this database have taken the Histel and Histosol delineations to be synonymous with peatlands. The fourth map is the wetland layer (GLWD-3, excluding the rivers and lakes of area > 1 km<sup>2</sup> of layers GLWD-1 and GLWD-2) of the Global Lakes and Wetland Database (GLWD; Lehner and Döll, 2004), in which wetland extents are the union of polygons from four different global databases.

Two global time-varying surface water products derived from remote-sensing observations were also examined in this study: the Global Inundation Extent from Multi-Satellites (GIEMS; Prigent et al., 2007; Papa et al., 2010), derived

**Table 1.** Observations and inversions used in this study.

Name	Reference	Description	Temporal domain	Temporal resolution	Spatial domain	Spatial resolution
<b>Wetland maps</b>						
Sheng2004	Sheng et al. (2004)	Wetland map of WSL based on digitization of regional maps of Markov (1971), Matukhin and Danilov (2000), and Romanova et al. (1977). Supplemented with peat cores.	Second half of 20th century	Static map	Western Siberia	1 : 2 500 000 north of 65° N, 1 : 1 000 000 south of 65° N
Peregono2008	Peregono et al. (2008)	Wetland map of WSL based on digitization of regional map of Romanova et al. (1977). Wetland types identified by remote sensing and field validation.	Second half of 20th century	Static map	Western Siberia	1 : 2 500 000
Northern Circumpolar Soil Carbon Database (NCSCD)	Tarnocai et al. (2009)	Map of wetlands across the northern circumpolar permafrost region. Over the WSL, based on maps of Fridland (1988) and Naumov (1993).	Second half of 20th century	Static map	Northern circumpolar permafrost region	1 : 2 500 000
Global Lake and Wetland Database (GLWD)	Lehner and Döll (2004)	Global lake and wetland map. Wetlands were the union of four global data sets.	Second half of 20th century	Static map	Global	1 : 1 000 000
<b>Surface Water</b>						
Global Inundation Extent from Multi-Satellites (GIEMS)	Papa et al. (2010)	Remote-sensing inundation product based on visible (AVHRR) and active (SSM/I) and passive (ERS) microwave sensors.	1993–2004	Daily, aggregated to monthly	Global	25 km equal-area grid, aggregated to 0.5° × 0.5°
Surface Water Microwave Product Series (SWAMPS)	Schroeder et al. (2010)	Remote-sensing inundation product based on active (SeaWinds-on-QuikSCAT, ERS, and ASCAT) and passive (SSM/I, SSM/I/S) microwave sensors.	1992–2013	Daily, aggregated to monthly	Global	25 km equal-area grid, aggregated to 0.5° × 0.5°
<b>CH<sub>4</sub> Inventory</b>						
Glagolev2011	Glagolev et al. (2011)	In situ flux sampling along transect spanning West Siberia, 2006–2010; statistical model of fluxes as function of wetland type applied to map of Peregono et al. (2008).	2006–2010	Monthly climatology	Western Siberia	0.5° × 0.5°
<b>CH<sub>4</sub> Inversions</b>						
Bloom2010	Bloom et al. (2010)	Global optimization of relationship between SCIAMACHY atmospheric CH <sub>4</sub> concentrations (Bovensmann et al., 1999), NCEP/NCAR surface temperatures (Kalnay et al., 1996), and GRACE gravity anomalies (Tapley et al., 2004).	2003–2007	Annual	Global	3° × 3°
Bousquet2011R	Bousquet et al. (2011), Bousquet et al. (2006)	Global inversion using LMDZ with Matthews and Fung (1987) inventory as the wetland prior.	1993–2009	Monthly	Global	1° × 1° resolution for prior, multiplied by single coefficient for all of boreal Asia
Bousquet2011K	Bousquet et al. (2011), Bousquet et al. (2006)	Global inversion using LMDZ with emissions from Kaplan (2002) as the wetland prior.	1993–2009	Monthly	Global	1° × 1° resolution for prior, multiplied by single coefficient for all of boreal Asia
Kim2011	Kim et al. (2011)	Global inversion, with Glagolev et al. (2010) as prior in WSL and with Fung et al. (1991) elsewhere.	2002–2007	Monthly climatology	Regional	1° × 1° resolution for prior, multiplied by single coefficient for all of WSL
Winderlich2012	Winderlich (2012), Schuldt et al. (2013)	Regional inversion over West Siberia, with Kaplan (2002) as the wetland prior.	2009	Monthly climatology	Regional	1° × 1° resolution for both prior and coefficients over WSL

from visible and near-infrared (AVHRR) and active (SSM/I) and passive (ERS) microwave sensors over the period 1993–2004, and the Surface Water Microwave Product Series (SWAMPS; Schroeder et al., 2010), derived from active (SeaWinds-on-QuikSCAT, ERS, and ASCAT) and passive (SSM/I, SSMI/S, AMSR-E) microwave sensors over the period 1992–2013. For both products, surface water area fractions ( $F_w$ ) were aggregated from their native 25 km equal-area grids to a  $0.5^\circ \times 0.5^\circ$  geographic grid and from daily to monthly temporal resolution, for consistency with model results.

For  $\text{CH}_4$  emissions, our primary reference for in situ observations was the estimate of Glagolev et al. (2011), which we will refer to as “Glagolev2011”. The Glagolev2011 product consists of both a database of over 2000 individual chamber observations from representative landforms at each of 36 major sites over the period 2006–2010 (Fig. 1a) and a map of long-term average emissions created by applying the mean observed emissions to the wetlands of the Peregon2008 map as a function of wetland type. It is worth noting that the Glagolev2011 product is currently undergoing a revision based on higher-resolution maps, which will lead to a substantial increase in annual emissions from the taiga zone, due to a larger spatial extent of high-emitting wetland types (Glagolev et al., 2013). Possible changes to emissions in the tundra zone (in the northern half of the WSL) are not yet known. We consider this product’s large uncertainty in our evaluation of model predictions.

We also considered emissions estimates from five inversions. Two of them were regional: “Kim2011” (Kim et al., 2011) and “Winderlich2012” (Winderlich, 2012; Schuldt et al., 2013). Kim et al. (2011) used an earlier version of Glagolev2011 (Glagolev et al., 2010) at a  $1^\circ \times 1^\circ$  resolution as their prior distribution for wetland emissions within the atmospheric transport model NIES-TM (Maksyutov et al., 2008) over the period 2002–2007. Kim et al. (2011) derived 12 climatological average monthly (spatially uniform) coefficients for wetland emissions to optimize atmospheric  $\text{CH}_4$  concentrations over the WSL relative to observed  $\text{CH}_4$  concentrations obtained by aircraft sampling at two locations in the WSL. Winderlich (2012) used the Kaplan (2002) wetland inventory for prior wetland emissions, within the global inversion system TM3-STILT (Rödenbeck et al., 2009; Trusilova et al., 2010) for the year 2009. Winderlich (2012) derived 12 monthly coefficients for wetland emissions, uniquely for each point in a  $1^\circ \times 1^\circ$  grid, to optimize atmospheric  $\text{CH}_4$  concentrations over the WSL relative to the concentrations measured at the Zotino Tall Tower Observatory and three other  $\text{CH}_4$  tower observation sites (Demianskoe, Igrim, and Karasev) located between  $58$  and  $63^\circ$  N.

The other inversions we considered were global: the “Reference” and “Kaplan” versions of the Bousquet et al. (2011) inversion, denoted by “Bousquet2011R” and “Bousquet2011K”, respectively, and the estimate of Bloom et al. (2010), denoted by “Bloom2010”. Bousquet et

al. (2011) used the Laboratoire de Météorologie Dynamique general circulation model (LMDZ; Hauglustaine et al., 2004) atmospheric transport model on a  $3.75^\circ \times 2.5^\circ$  grid to estimate monthly  $\text{CH}_4$  emissions at a  $1^\circ \times 1^\circ$  resolution for the period 1993–2009, optimizing atmospheric concentrations of several gases, including  $\text{CH}_4$ , relative to global surface observation networks, for both inversions. The Matthews and Fung (1987) emissions inventory was the prior for wetland emissions in the Bousquet2011R inversion, while the Kaplan (2002) emissions were the prior for the Bousquet2011K inversion. In both cases, a single, spatially uniform set of monthly coefficients was derived for each of 11 large regions of the globe. The region containing the WSL was boreal Asia (in which the WSL makes up the majority of the wetlands). Consequently, spatial patterns in estimated emissions at the scale of  $1^\circ \times 1^\circ$  were identical to those of the prior emissions; only the regional total emissions were constrained by the inversions. The 17-year record length of the Bousquet2011 inversions made them appealing candidates for investigating the sensitivities of emissions to interannual variability in environmental drivers. Bloom et al. (2010) did not use an atmospheric transport model, but rather optimized the parameters in a simple model relating observed atmospheric  $\text{CH}_4$  concentrations from the Scanning Imaging Absorption Spectrometer for Atmospheric Chemistry (SCIAMACHY; Bovensmann et al., 1999) on the Envisat satellite to observed surface temperatures from the National Center for Environmental Prediction/National Center for Atmospheric Research (NCEP/NCAR) weather analyses (Kalnay et al., 1996) and gravity anomalies from the Gravity Recovery and Climate Experiment satellite (GRACE; Tapley et al., 2004), under the assumption that gravity anomalies are indicative of large-scale surface and near-surface water anomalies. The Bloom2010 inversion covered the period 2003–2007, at a  $3^\circ \times 3^\circ$  resolution.

## 2.4 Models

Among the participating models (Table 2) were those of the WETCHIMP study (Melton et al., 2013; Wania et al., 2013) that contributed  $\text{CH}_4$  emissions estimates: CLM4Me (Riley et al., 2011), DLEM (Tian et al., 2010, 2011a, b, 2012), IAP-RAS (Mokhov et al., 2007; Eliseev et al., 2008), LPJ-Bern (Spahni et al., 2011, Zürcher et al., 2013), LPJ-WHyMe (Wania et al., 2009a, b, 2010), LPJ-WSL (Hodson et al., 2011), ORCHIDEE (Ringeval et al., 2010), SDGVM (Hopcroft et al., 2011), and UW-VIC (denoted by “UW-VIC (GIEMS)”); Bohn et al., 2013). In addition, we analyzed several other models. “UW-VIC (SWAMPS)” is another instance of UW-VIC with surface water calibrated to match the SWAMPS product. VISIT (Ito and Inatomi, 2012) contributed four configurations using different combinations of wetland maps and methane models: “VISIT (GLWD)” and “VISIT (Sheng)” used the Cao (1996) methane model with the GLWD and Sheng2004 wetland maps, respectively,



and “VISIT (GLWD-WH)” and “VISIT (Sheng-WH)” replaced the Cao model with the Walter and Heimann (2000) model. LPX-BERN (Spahni et al., 2013; Stocker et al., 2013, 2014) is a newer version of LPJ-Bern that also contributed four configurations: “LPX-BERN”, which prescribed peatland extent using Peregón2008 and inundation extent using GIEMS; “LPX-BERN (DyPTOP)”, which dynamically predicted the extents of peatlands and inundation; and “LPX-BERN (N)” and “LPX-BERN (DyPTOP-N)”, which additionally simulated interactions between the carbon and nitrogen cycles. DLEM2 is a newer version of DLEM that includes soil thermal physics and lateral matter fluxes (Liu et al., 2013; Pan et al., 2014). LPJ-MPI (Kleinen et al., 2012) is a version of the LPJ model that contains a dynamic peatland model with methane transport by the model of Walter and Heimann (2000). Finally, VIC-TEM-TOPMODEL (Zhu et al., 2014) is a hybrid of UW-VIC (Liang et al., 1994), TEM (Zhuang et al., 2004), and TOPMODEL (Beven and Kirkby, 1979).

The relevant hydrologic and biogeochemical features of these models are listed in Tables 2 and 3, respectively. The models used a variety of approaches to define CH<sub>4</sub>-producing areas. To have some consistency across models, the original WETCHIMP study asked participating modelers to use the GIEMS product if their model required wetland extent to be prescribed. Accordingly, some models (DLEM, DLEM2, and LPJ-WSL) used the GIEMS surface water product exclusively to prescribe (time-varying) CH<sub>4</sub>-producing areas; these are denoted by the code “S” in Table 2.

Several models (CLM4Me, LPJ-MPI, LPX-BERN (DyPTOP), LPX-BERN (DyPTOP-N), ORCHIDEE, SDGVM, and VIC-TEM-TOPMODEL) predicted surface water and CH<sub>4</sub>-producing areas dynamically using topographic information and the TOPMODEL (Beven and Kirkby, 1979) distributed water table approach (in which the area over which the water table is at or above the soil surface can be interpreted to correspond to surface water extent); these models are denoted by a “T” in Table 2. For these models, the CH<sub>4</sub>-producing area is the area in which labile soil carbon is sufficiently warm and anoxic for methanogenesis to occur, including both surface water and any non-inundated land with sufficiently shallow water table depths. LPJ-MPI and LPX-BERN (DyPTOP and DyPTOP-N) prognostically determined peatland area as a function of long-term soil moisture conditions; their CH<sub>4</sub>-producing areas thus included peatlands (inundated or not) as well as completely saturated or inundated mineral soils. Because the other T models’ CH<sub>4</sub>-producing areas had no explicit limits, those teams reported approximations of the models’ true CH<sub>4</sub>-producing areas: CLM4Me, ORCHIDEE, and VIC-TEM-TOPMODEL reported their surface water areas; and SDGVM reported the area for which the water table was above a threshold depth, with the threshold chosen to minimize the global rms error between this area and GIEMS. Additionally, both CLM4Me

and ORCHIDEE tied their surface water areas to the long-term mean of GIEMS: CLM4Me did so by calibration and ORCHIDEE did so by rescaling its surface water areas. Thus, we have placed these two models in the S category in Table 2.

Finally, the remaining models (IAP-RAS, LPJ-Bern, LPJ-WHyMe, LPX-BERN, LPX-BERN (N), both UW-VIC configurations, and all four VISIT configurations) used wetland maps, either alone or in combination with topography and surface water products, to inform their wetland schemes; these are denoted by “M” in Table 2. In most cases, the wetland maps were used to determine the maximum extent of the CH<sub>4</sub>-producing area, within which inundated area and water table depths would vary in time. In contrast, LPJ-Bern, LPX-BERN, and LPX-BERN (N) allowed inundated area (specified by GIEMS) to sometimes exceed the static map-based peatland area; in such cases, it was assumed that the excess inundation occurred in mineral soils. Thus, the CH<sub>4</sub>-producing area included peatlands and inundated mineral soils. LPJ-Bern additionally allowed CH<sub>4</sub> production in areas of “wet mineral soil” (in which soil moisture content was greater than 95 % of water-holding capacity) and included this in the total CH<sub>4</sub>-producing area.

Models’ hydrologic approaches varied in other ways as well. Some (IAP-RAS and LPJ-WSL) did not include explicit water table depth formulations for estimating emissions in unsaturated (non-inundated) wetlands; IAP-RAS assumed all wetlands were completely saturated, and LPJ-WSL only considered unsaturated wetlands implicitly, using soil moisture as a proxy. Most of the other models used a TOPMODEL approach to relate the distribution of water table depths across the grid cell to topography (generally on a 1 km scale). However, LPJ-WHyMe, UW-VIC (GIEMS), and UW-VIC (SWAMPS) determined water table depth distributions within peatlands from assumed proportions of microtopographic landforms (e.g., hummocks and lawns) on the (horizontal) scale of meters. UW-VIC explicitly handled lakes by treating lakes and peatlands as a single system, spanning the total area of lakes and peatlands which was given by the Sheng et al. (2004) data set and within which surface water area varied dynamically. Areas of permanent surface water over the period 1949–2010 were considered to be lakes and were excluded from methane emissions estimates.

Models also varied in their soil thermal physics schemes. Most models used a one-dimensional heat diffusion scheme to determine the vertical profile of soil temperatures, but VISIT used a linear interpolation between current air temperature (at the soil surface) and annual average air temperature (at the bottom of the soil column). Several models (DLEM, LPJ-MPI, LPJ-WSL, and SDGVM) did not consider the water-ice phase change and therefore did not model permafrost. While IAP-RAS contained a permafrost scheme, it was driven by seasonal and annual summaries of meteorological forcings and used simple analytic functions to estimate the seasonal evolution and vertical profile of soil temperatures. Additionally, DLEM and LPJ-WSL did not con-



**Table 3.** Participating models and their relevant biogeochemical features.

Model	$R_{\text{anaerobic}}/R_{\text{aerobic}}^1$	C substrate source <sup>2</sup>	pH <sup>3</sup>	Redox state <sup>4</sup>	Dynamic vegetation <sup>5</sup>	Nitrogen–carbon cycle interaction <sup>6</sup>	Saturated NPP inhibition <sup>7</sup>	Parameter selection <sup>8</sup>
CLM4Me	Variable	Cpool	Yes	Yes	Yes	Yes	No	Optimized to various sites
DLEM	Variable	NPP and Cpool	Yes	Yes	No	No	No	Optimized to various sites
DLEM2	Variable	NPP and Cpool	Yes	Yes	No	No	No	Optimized to various sites
IAP-RAS	n/a	Cpool	No	No	No	No	No	Literature; scaled to global total
LPJ-Bern	Constant	NPP and Cpool	No	No	Yes	No	Yes	Optimized to various sites; scaled to global total
LPJ-MPI	Constant	Cpool	No	No	Yes	No	Yes	Literature
LPJ-WHyMe	Constant	NPP and Cpool	No	No	Yes	No	Yes	Literature; scaled to global total
LPJ-WSL	Constant	Cpool	No	No	Yes	No	No	Literature
LPX-BERN	Constant	NPP and Cpool	No	No	Yes	No	Yes	Optimized to various sites; scaled to global total
LPX-BERN (DyPTOP)	Constant	NPP and Cpool	No	No	Yes	No	Yes	Optimized to various sites; scaled to global total
LPX-BERN (N)	Constant	NPP and Cpool	No	No	Yes	Yes	Yes	Optimized to various sites; scaled to global total
LPX-BERN (DyPTOP-N)	Constant	NPP and Cpool	No	No	Yes	Yes	Yes	Optimized to various sites; scaled to global total
ORCHIDEE	Variable	Cpool	No	No	Yes	No	No	Literature and optimized to various sites
SDGVM	Variable	Cpool	No	No	Yes	No	No	Literature
UW-VIC(GIEMS)	Variable	NPP	No	No	No	No	Yes	Optimized to sites in Glagolev2011
UW-VIC(SWAMPS)	Variable	NPP	No	No	No	No	Yes	Optimized to sites in Glagolev2011
VIC-TEM-TOPMODEL	Variable	NPP	Yes	Yes	No	No	No	Optimized to various sites
VISIT(GLWD)	Variable	Cpool	No	No	No	Yes (only affects upland CH <sub>4</sub> oxidation)	No	Literature
VISIT(GLWD-WH)	Variable	NPP	No	No	No	Yes (only affects upland CH <sub>4</sub> oxidation)	No	Literature
VISIT(Sheng)	Variable	Cpool	No	No	No	Yes (only affects upland CH <sub>4</sub> oxidation)	No	Literature
VISIT(Sheng-WH)	Variable	NPP	No	No	No	Yes (only affects upland CH <sub>4</sub> oxidation)	No	Literature

<sup>1</sup>  $R_{\text{anaerobic}}/R_{\text{aerobic}}$ : how the ratio of anaerobic to aerobic respiration is handled in the model (constant: ratio is held constant; variable: ratio varies either as an explicit function of environmental conditions or as the result of separate governing equations for aerobic and anaerobic respiration; n/a: not applicable).

<sup>2</sup> Carbon substrate source: Cpool: soil carbon pool; NPP: root exudates, in proportion to net primary productivity.

<sup>3</sup> pH: indicates whether soil pH influences CH<sub>4</sub> emissions.

<sup>4</sup> Redox state: indicates whether soil redox state influences CH<sub>4</sub> emissions.

<sup>5</sup> Dynamic vegetation: indicates whether vegetation species abundances change in response to environmental conditions.

<sup>6</sup> Nitrogen–carbon cycle interaction: indicates whether interactions between the nitrogen and carbon cycles influence CH<sub>4</sub> emissions.

<sup>7</sup> Saturated NPP inhibition: indicates whether NPP decreases under wet soil conditions for any plant species.

<sup>8</sup> Parameter selection: method of choosing parameter values (literature: values chosen from ranges reported in literature; optimized: values chosen to minimize the difference between simulated and observed values, either of CH<sub>4</sub> fluxes at selected sites or of global atmospheric CH<sub>4</sub> concentrations).

sider the insulating effects of organic (peat) soil. In contrast, UW-VIC modeled permafrost, peat soils, and the dynamics of surface water, including lake ice cover and evaporation, thereby adding another factor that influences soil temperatures.

Models also varied in their biogeochemical schemes (Table 3). Most represented methane production as a function of soil temperature, water table depth (except for IAP-RAS and LPJ-WSL), and the availability of carbon substrate. Most (except for IAP-RAS and LPJ-WSL) explicitly accounted for the oxidation of methane above the water table; and most accounted for some degree of plant-aided transport. Some models (LPJ-Bern, LPJ-MPI, LPJ-WHyMe, and LPX-BERN) represented methane production as either a constant or soil-moisture-dependent fraction of aerobic respiration. Some models (DLEM, DLEM2, and VIC-TEM-TOPMODEL) imposed additional dependences on soil pH and oxidation state. Models differed in the pathways and availability of carbon substrate: some models (UW-VIC, VIC-TEM-TOPMODEL, VISIT (GLWD-WH), and VISIT (Sheng-WH)) related carbon substrate availability to net primary productivity (NPP) as a proxy for root exudates; some (CLM4Me, IAP-RAS, LPJ-MPI, LPJ-WSL, ORCHIDEE,

SDGVM, VISIT (GLWD), and VISIT (Sheng)) related carbon substrate to the content and residence times of various soil carbon reservoirs; and others (DLEM, DLEM2, LPJ-Bern, LPJ-WHyMe, all four LPX-BERN configurations) drew carbon substrate from a combination of both root exudates and soil carbon (or dissolved organic carbon, in the case of DLEM and DLEM2). CLM4Me and two configurations of LPX-BERN simulated interactions between the carbon and nitrogen cycles. Several models (all versions of LPJ and LPX, ORCHIDEE, and SDGVM) included dynamic vegetation components. Some models (LPJ-Bern, LPJ-MPI, LPJ-WHyMe, LPX-BERN, and UW-VIC) accounted for the inhibition of NPP of some plant species under saturated soil moisture conditions. Finally, models employed a variety of methods, alone or in combination (Table 3), to select parameter values, including taking the median of literature values, optimizing emissions to match in situ observations from representative sites regionally (e.g., UW-VIC optimized parameter values to match the Glagolev2011 data set in the WSL) or globally, or optimizing global total emissions to match various estimates from inversions.

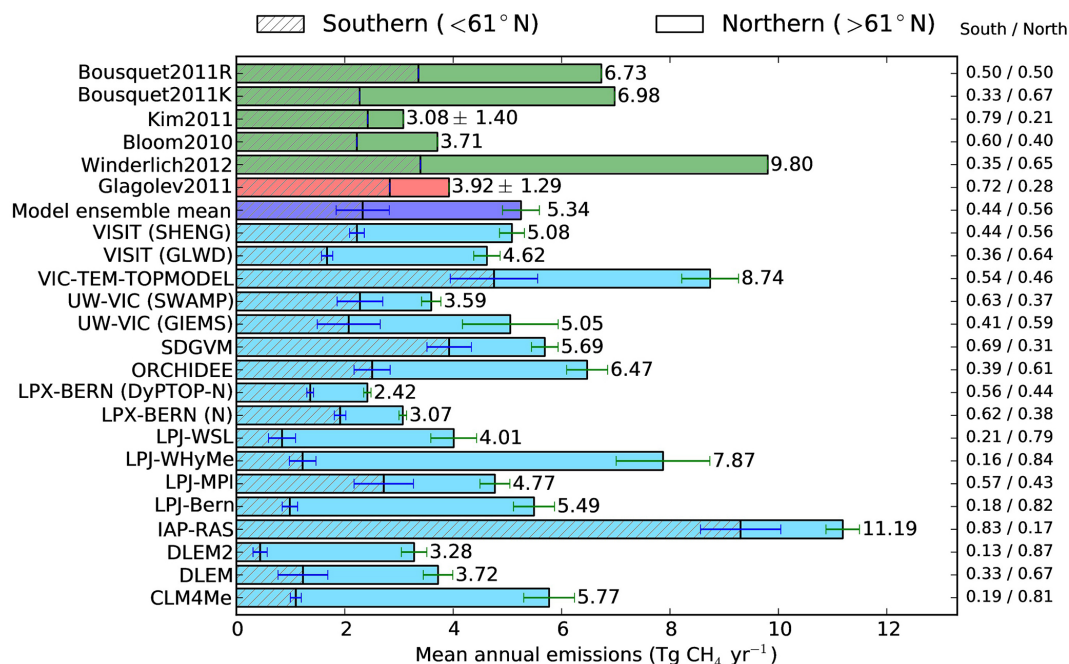


**Figure 2.** Mean annual emissions from the WSL: from inversions (green), observation-based estimates (red), and forward models (blue). The hatched portions of the bars indicate the emissions from the southern half of the domain (latitude  $< 61^\circ \text{N}$ ). Error bars on the model results indicate the interannual standard deviations of the southern and northern emissions. Error bars on the inversions and observational estimates indicate the uncertainty given in those studies. Numeric fractions of the total emissions contributed by the southern and northern halves of the domain are displayed in the right-hand column.

## 2.5 Model simulations

To be consistent with WETCHIMP's transient simulation ("Experiment 2-trans", Wania et al., 2013), we focused our analysis on the period 1993–2004, although several non-WETCHIMP models provided data from 1993–2010. All models used the CRUNCEP gridded meteorological forcings (Viovy and Ciais, 2011) as a common input. Model-specific inputs are described in Wania et al. (2013).

Model outputs (monthly CH<sub>4</sub> emissions (average g CH<sub>4</sub> month<sup>-1</sup> m<sup>-2</sup> over the grid cell area) and monthly CH<sub>4</sub>-producing area (km<sup>2</sup>)) were analyzed at a  $0.5^\circ \times 0.5^\circ$  spatial resolution (resampled from native resolution as necessary).

Due to large seasonal variations in CH<sub>4</sub>-producing areas, our analysis focused on June–July–August (JJA) averages of area and CH<sub>4</sub> emissions, since it is during these months that the majority of the year's methane is emitted across all models (areas in other seasons would not be representative of annual CH<sub>4</sub> emissions). Similarly, in analyzing interannual variability in CH<sub>4</sub> emissions, we focused on JJA CH<sub>4</sub> emissions, which dominate the annual total and have stronger correlations with JJA environmental factors (such as air temperature, precipitation, or inundation) than annual CH<sub>4</sub> emissions have with annual average environmental factors. We also computed growing season CH<sub>4</sub> "intensities" (average JJA CH<sub>4</sub> emissions per unit JJA CH<sub>4</sub>-producing area).

## 2.6 Data access

All data used in this study, including observational products, inversions, and forward model results, are available from WETCHIMP-WSL (2015).

## 3 Results

### 3.1 Average annual total emissions

As shown in Fig. 2 and Table S1 in the Supplement, 12-year mean estimates ( $\pm$ standard error on the mean) of annual total emissions over the WSL from forward models ( $5.34 \pm 0.54 \text{ Tg CH}_4 \text{ yr}^{-1}$ ), inversions ( $6.06 \pm 1.22 \text{ Tg CH}_4 \text{ yr}^{-1}$ ), and observations ( $3.91 \pm 1.29 \text{ Tg CH}_4 \text{ yr}^{-1}$ ) largely agreed, despite large scatter in individual estimates. Model estimates ranged from 2.42 (LPX-BERN (DyPTOP-N)) to  $11.19 \text{ Tg CH}_4 \text{ yr}^{-1}$  (IAP-RAS). The Glagolev2011 estimate was substantially lower than the mean of the models, corresponding to the 36th percentile of the distribution of model estimates. However, the potential upward revision of Glagolev2011 (Sect. 2.2) would move it to a substantially higher percentile of their distribution. Inversions yielded a similarly large range of estimates: 3.08 (Kim2011) to  $9.80 \text{ Tg CH}_4 \text{ yr}^{-1}$  (Winderlich2012). Despite their large spread, 15 out of

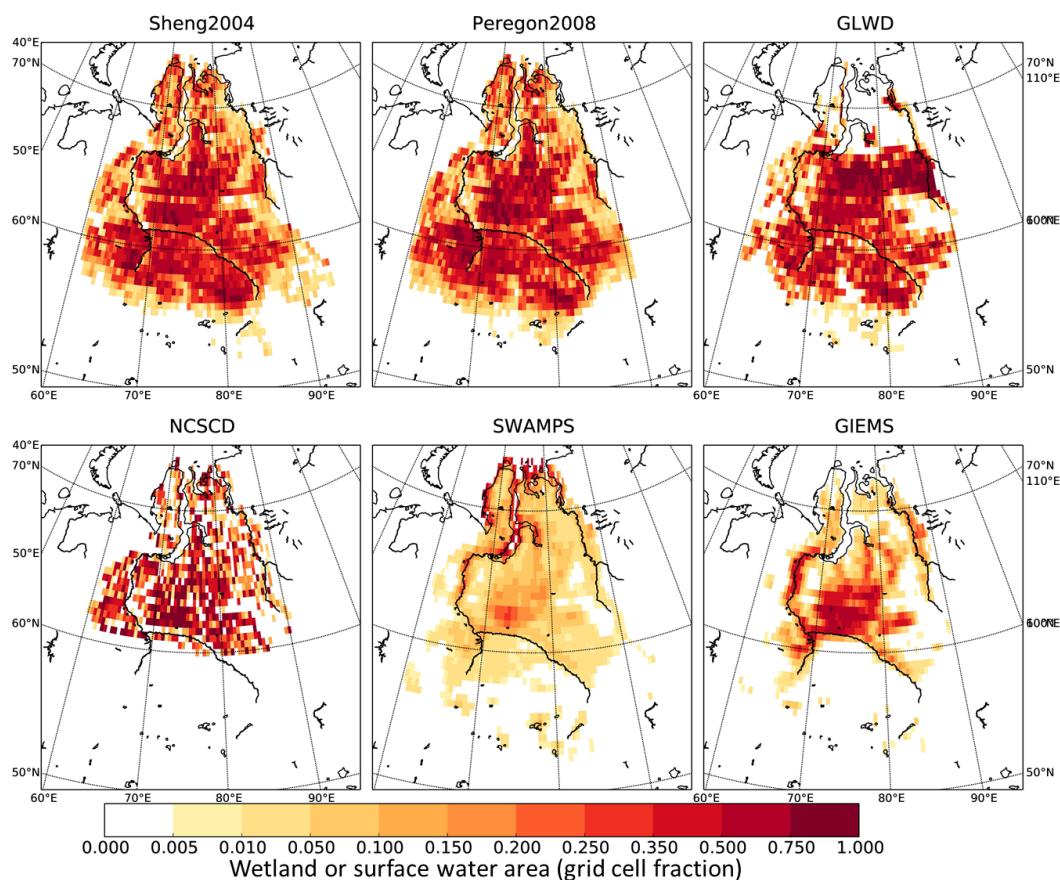


**Figure 3.** Observational data sets related to wetland areas. For SWAMPS and GIEMS, areas shown are the June–July–August (JJA) average surface water area fraction over the period 1993–2004.

the 17 forward models fell within the range of inversion estimates. Here we have excluded the “WH” configurations of VISIT and the configurations of LPX-BERN for which nitrogen–carbon interaction was turned off, due to their similarities to their counterparts that were included. The wide variety in the relative proportions of  $\text{CH}_4$  emitted from the south and north halves of the domain, with the southern contribution ranging from 13 to 69% (right-hand column in Fig. 2), indicates a lack of agreement on which types of wetlands and climate conditions are producing the bulk of the region’s  $\text{CH}_4$ .

### 3.2 Differences among observational data sets

The large degree of disagreement among observational data sets is worth addressing before using them to evaluate the models. Important differences are evident among wetland maps (Fig. 3). Sheng2004 and Peregon2008 are extremely similar, in part because they both used the map of Romanova (1977) north of 65° N. Both of these data sets show wetlands distributed across most of the WSL, with large concentrations south of the Ob’ River (55–61° N, 70–85° E), east of the confluence of the Ob’ and Irtysh rivers (57–62° N, 65–

70° E), and north of the Ob’ River (61–66° N, 70–80° E). In comparison, the GLWD map entirely lacks wetlands in the tundra region north of 67° N and shows additional wetland area in the northeast (64–67° N, 70–90° E). The NCSCD is substantially different from the other three maps. Owing to its focus on permafrost soils, it completely excludes the extensive wetlands south of the southern limit of permafrost (approximately 60° N). Given the numerous field studies documenting these productive southern wetlands (Sect. 2.1), the NCSCD seems to be inappropriate for studies that extend beyond permafrost.

The two surface water products (GIEMS and SWAMPS) also exhibit large differences. While they both agree that the surface water area fraction ( $F_w$ ) is most extensive in the central region north of the Ob’ River (61–64° N), GIEMS gives areal extents that are 3–6 times those of SWAMPS. Outside of this central peak, GIEMS  $F_w$  drops off rapidly to nearly 0 in most places (particularly in the forested region south of the Ob’ River, which may be due to difficulties in detecting inundation under vegetative canopy and/or reduced sensitivity where the open-water fraction is less than 10%; Prigent et al., 2007), while SWAMPS maintains low levels of  $F_w$  through-

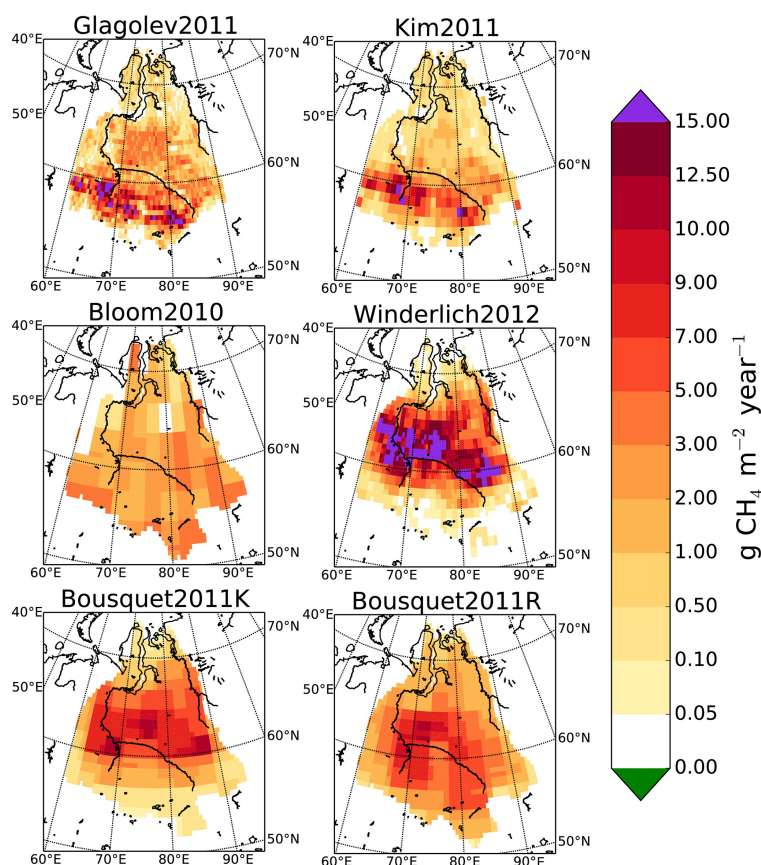


**Figure 4.** Observation- and inversion-based estimates of annual  $\text{CH}_4$  emissions ( $\text{g CH}_4 \text{ yr}^{-1} \text{ m}^{-2}$  of grid cell area). For inversions, averages are over the following periods: 2002–2007 (Kim2011), 2003–2007 (Bloom2010), 2009 (Winderlich2012), and 1993–2004 (Bousquet2011K and R).

out most of the WSL. Along the Arctic coastline, SWAMPS shows high  $F_w$ , which may indicate contamination of the signal by the ocean. In both data sets,  $F_w$  exhibits some similarity with the distribution of lakes and rivers (Fig. 1), illustrating the inclusion of non-wetlands in these surface water products.

Among the  $\text{CH}_4$  data sets (Fig. 4), a clear difference can be seen between the spatial distributions of Glagolev2011 and Kim2011 (both of which assign the majority of emissions to the region south of the Ob’ River, between 55 and 60° N); and Winderlich2012 and Bousquet2011K (both of which assign the majority of emissions to the central region north of the Ob’ River, between 60 and 65° N). We discuss possible reasons for this discrepancy in Sect. 4.3. The global inversions (Bousquet2011R and K, and Bloom2010) have coarser spatial resolution than the regional inversions of Kim2011 and Winderlich2012. Bousquet2011R and K have similar distributions between 60 and 65° N, but Bousquet2011R has relatively stronger emissions between 57 and 60° N and weaker emissions between 65 and 67° N; in this respect, Bousquet2011R is intermediate between Glagolev2011 and Winderlich2012. Finally, Bloom2010 exhibits relatively lit-

tle spatial variability in emissions, likely due to its use of GRACE observations as a proxy for wetland inundation and water table conditions.

### 3.3 Primary drivers of model spatial uncertainty

The wide disagreement among models is plainly evident in Fig. 5, which plots average JJA  $\text{CH}_4$  emissions versus average JJA  $\text{CH}_4$ -producing areas for the WSL as a whole (top left), the south (bottom left), and the north (bottom right). A series of lines (“spokes”) passing through the origin, with slopes of integer multiples of  $1 \text{ g CH}_4 \text{ m}^{-2} \text{ month}^{-1}$ , allows comparison of spatial average intensities ( $\text{CH}_4$  emissions per unit  $\text{CH}_4$ -producing area). All points along a given line have the same intensity but different  $\text{CH}_4$ -producing areas. We have included the Glagolev2011–Peregon2008  $\text{CH}_4$ –area estimate (denoted by a black star) and the mean of the inversions (denoted by a grey star) for reference. We set the area coordinate for the inversions to Peregon2008 because (a) the wetland area was not available for all inversions and (b) Peregon2008 is a relatively accurate estimate of wetland area. JJA  $\text{CH}_4$  emissions, JJA wetland or  $\text{CH}_4$ -producing areas, and JJA intensities, for all models, observations, and inversions,

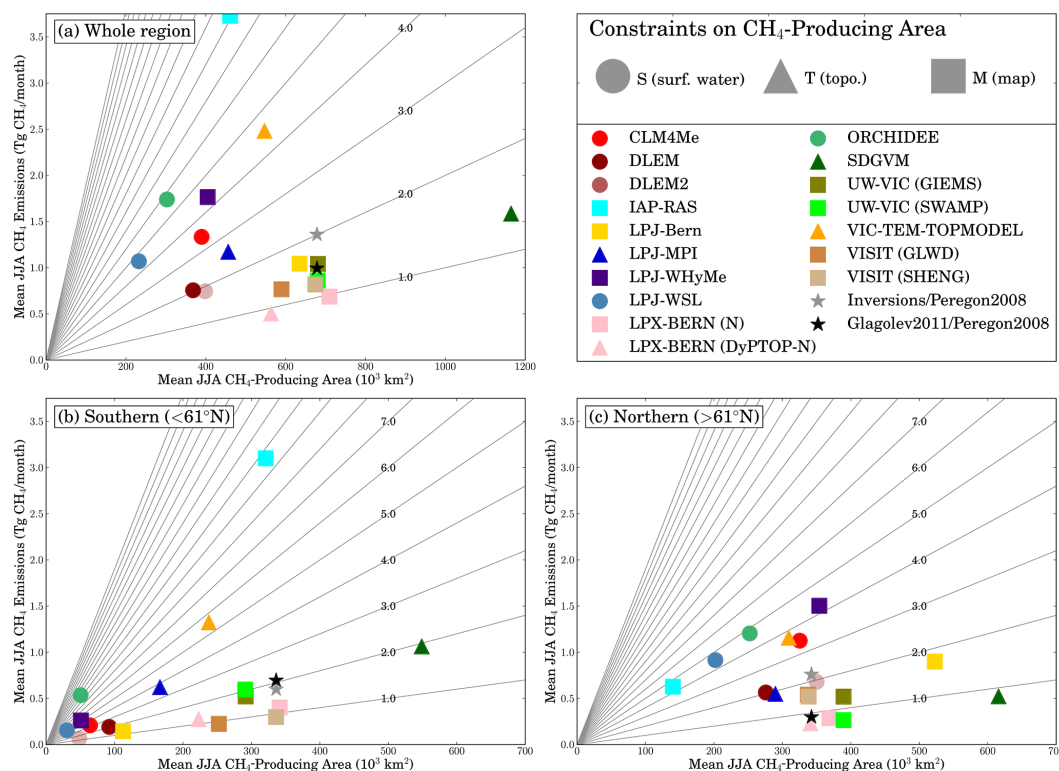


**Figure 5.** Model estimates of JJA CH<sub>4</sub> emissions (Tg CH<sub>4</sub> month<sup>-1</sup>) and JJA wetland or CH<sub>4</sub>-producing area (10<sup>3</sup> km<sup>2</sup>): for the entire WSL (top left) and the southern (bottom left) and northern (bottom right) halves, for the period 1993–2004. Lines passing through the origin, with slopes of integer multiples of 1 g CH<sub>4</sub> m<sup>-2</sup> month<sup>-1</sup>, allow a comparison of spatial average intensities (CH<sub>4</sub> emissions per unit CH<sub>4</sub>-producing area). Circles denote models that used satellite surface water products alone (corresponding to code S in Table 2) to delineate wetlands. Triangles denote models that used topographic information, with or without surface water products (corresponding to code T in Table 2). Squares denote models that used wetland maps with or without topography or surface water products (corresponding to code M in Table 2).

**Table 4.** Estimates of June–July–August CH<sub>4</sub> emissions from subsets of the participating models, over the entire WSL and its southern (< 61° N) and northern halves, for the period 1993–2004. Biases were computed with respect to the Glagolev2011–Peregon2008 estimates.

Subset	Average Jun–Jul–Aug CH <sub>4</sub> (Tg CH <sub>4</sub> month <sup>-1</sup> )									Average Jun–Jul–Aug contributing area (10 <sup>3</sup> km <sup>2</sup> )								
	WSL			South			North			WSL			South			North		
	Mean	Bias	SD	Mean	Bias	SD	Mean	Bias	SD	Mean	Bias	SD	Mean	Bias	SD	Mean	Bias	SD
I	1.10	0.14	0.37	0.22	-0.45	0.16	0.89	0.59	0.24	388	-291	136	66	-270	31	321	-21	112
T	1.42	0.46	0.82	0.81	0.14	0.46	0.61	0.31	0.39	682	4	325	294	-42	173	389	46	153
M	1.32	0.36	1.01	0.69	0.02	0.97	0.64	0.34	0.40	605	-74	113	250	-87	109	355	12	105
M+	1.30	0.34	1.17	0.85	0.18	1.10	0.45	0.16	0.15	633	-46	93	306	-30	34	327	-15	95

are listed in Table S1. Over the entire WSL (Fig. 5, top left), the scatter in model estimates of CH<sub>4</sub> emissions results from scatter in both area (ranging from 200 000 to 1200 000 km<sup>2</sup>) and intensity (ranging from 1 to 8 g CH<sub>4</sub> m<sup>-2</sup> month<sup>-1</sup>), with no clear relationship between the two.

However, a strong area-driven bias is evident in the south (Fig. 5, bottom left). Although the mean modeled CH<sub>4</sub> emission rate (0.58 Tg CH<sub>4</sub> month<sup>-1</sup>) is fairly close to both Glagolev2011 (0.67 Tg CH<sub>4</sub> month<sup>-1</sup>) and the mean of inversions (0.60 Tg CH<sub>4</sub> month<sup>-1</sup>), the distribution of model

estimates is substantially skewed, with most models' estimates falling well below both Glagolev2011 and the mean of the inversions. Glagolev2011's estimate corresponds to the 81st percentile of the model CH<sub>4</sub> distribution; the expected upward revision of Glagolev2011 (Sect. 2.2; exact JJA amount not yet known) would only raise that percentile. The mean of the inversions corresponds to the 76th percentile. Similarly, the models substantially underestimate the CH<sub>4</sub>-producing area, with Peregon2008 occupying the 83rd percentile of the model distribution. On the other hand,

**Table 5.** Spatial correlations between simulated average annual CH<sub>4</sub> emissions and GIEMS surface water area fraction ( $F_w$ ).

Model	Correlation	Model	Correlation	Model	Correlation
CLM4Me	0.69	LPJ-WHyMe	0.45	UW-VIC (GIEMS)	0.44
DLEM	0.70	LPJ-WSL	0.97	UW-VIC (SWAMPS)	0.11
DLEM2	0.21	LPX-BERN (N)	0.41	VIC-TEM-TOPMODEL	0.41
IAP-RAS	-0.03	LPX-BERN (DyPTOP-N)	0.28	VISIT (GLWD)	0.62
LPJ-Bern	0.56	ORCHIDEE	0.61	VISIT (Sheng)	0.65
LPJ-MPI	0.01	SDGVM	0.09		

**Table 6.** Mean CH<sub>4</sub> emissions from LPX-BERN, 1993–2010, for the entire WSL and the south and north halves of the domain.

Configuration	Mean [Tg CH <sub>4</sub> yr <sup>-1</sup> ]		
	WSL	South	North
LPX-BERN	3.81	1.98	1.83
LPX-BERN (DyPTOP)	3.17	1.38	1.79
LPX-BERN (N)	3.08	1.92	1.17
LPX-BERN (DyPTOP-N)	2.44	1.37	1.08
Differences			
LPX-BERN (N) – LPX-BERN	-0.73	-0.06	-0.66
LPX-BERN (DyPTOP-N) – LPX_BERN (DyPTOP)	-0.73	-0.02	-0.71
LPX-BERN (DyPTOP) – LPX-BERN	-0.64	-0.60	-0.04
LPX-BERN (DyPTOP-N) – LPX-BERN (N)	-0.64	-0.55	-0.09

the model intensity distribution is much less biased, with Glagolev2011 corresponding to the 47th percentile. Even a doubling of Glagolev2011's intensity would place it at only the 69th percentile of the model distribution, a smaller bias than for area. Thus, the area bias is the major driver of CH<sub>4</sub> bias in the south. In comparison, the north (Fig. 5, bottom right) is relatively unbiased.

Model inputs and formulations played a key role in determining CH<sub>4</sub>-producing area biases. Statistics of model performance relative to Glagolev2011–Peregon2008, categorized by the wetland codes in Table 2, are listed in Table 4. The models that used satellite surface water products alone (denoted by circles in Fig. 5 and the code S in Table 2) estimated the lowest CH<sub>4</sub>-producing areas in the south, with a bias of -270 000 km<sup>2</sup> and standard deviation of 31 000 km<sup>2</sup>. Additionally, two models (LPJ-Bern and LPJ-WHyMe) from the M group (denoted by squares in Fig. 5 and the code M in Table 2) also yielded low areas, due to their use of the NCSCD map, which omitted non-permafrost wetlands. The “M+” group, consisting of all M models except those two, exhibited the smallest bias and second-smallest standard deviation (-31 000 and 34 000 km<sup>2</sup>, respectively). Models that determined CH<sub>4</sub>-producing area dynamically using topographic data but without the additional input of wetland maps (denoted by triangles in Fig. 5 and the code T in Table 2) yielded nearly as small a bias as the M+ group (-42 000 km<sup>2</sup>) but had the largest scatter (standard deviation of 173 000 km<sup>2</sup>) of the

groups. The fact that two of the S models (CLM4Me and ORCHIDEE) supplied CH<sub>4</sub>-producing areas that excluded non-inundated methane-emitting wetlands had little effect on the results, since their total CH<sub>4</sub> emissions (which included non-inundated emissions) also suffered from a large negative bias (-0.45 Tg CH<sub>4</sub> yr<sup>-1</sup>, or -67 %).

Examining the spatial distributions of annual CH<sub>4</sub> (Fig. 6) and JJA CH<sub>4</sub>-producing areas (Fig. 7) shows why the use of surface water data alone results in poor model performance. Among the models from the S group (CLM4Me, DLEM, DLEM2, LPJ-WSL, and ORCHIDEE), the spatial distributions of both CH<sub>4</sub> emissions and CH<sub>4</sub>-producing area tend to be strongly correlated with GIEMS (See Table 5 for correlations), which exhibits very low surface water areas south of the Ob' River, despite the large expanses of wetlands there (Sect. 3.2). Similarly, the low emissions of LPJ-WHyMe and LPJ-Bern in the south can be explained by their use of the NCSCD map, which only considered peatlands (Histels and Histosols) within the circumpolar permafrost zones (which only occur north of 60° N). For LPJ-WHyMe, these permafrost peatlands were the only type of wetland modeled (i.e., the model domain only included the circumpolar permafrost zones), so LPJ-WHyMe's emissions were almost nonexistent in the south. LPJ-Bern also used the NCSCD's Histels and Histosols to delineate peatlands but additionally simulated methane dynamics in wet or inundated mineral soils outside the permafrost zone. While this allowed LPJ-Bern to make emissions estimates in the south, the much

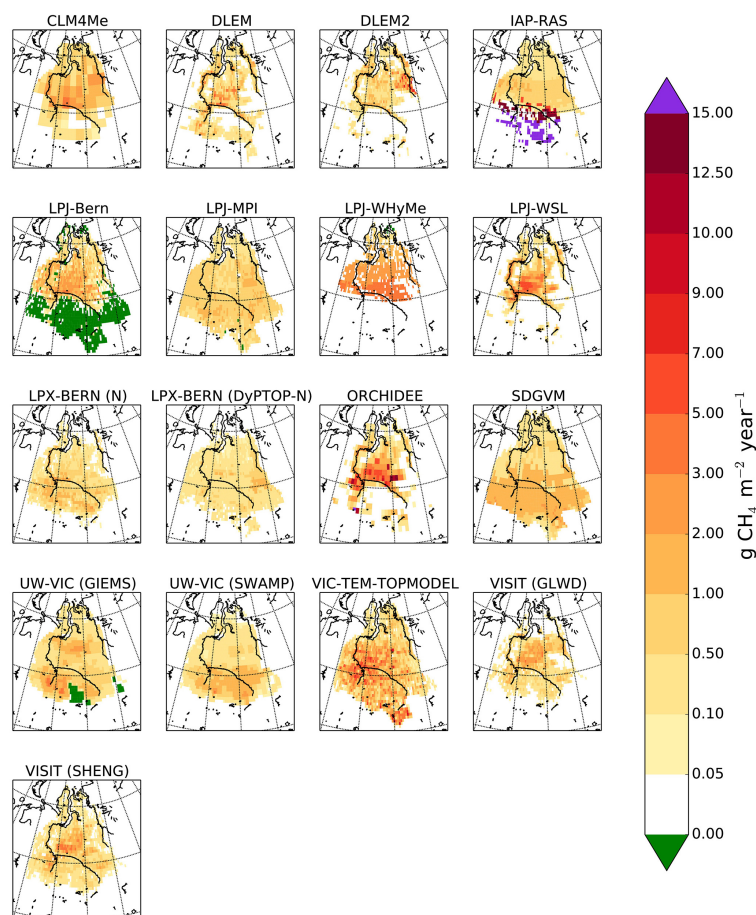


**Figure 6.** Maps of simulated average annual  $\text{CH}_4$  emissions ( $\text{g CH}_4 \text{ m}^{-2} \text{ yr}^{-1}$  of grid cell area).

lower porosities of mineral soils resulted in larger sensitivities of water table depth to evaporative loss than those of peat soils. These drier soils led to net  $\text{CH}_4$  oxidation in much of the south.

Aside from area-driven biases, a large degree of intensity-driven scatter is evident in both the south and north. Indeed, the underestimation of areas in the south, accompanied by resulting reductions in  $\text{CH}_4$  emissions, partially compensated for some of the intensity-driven scatter there. However, some of the more extreme intensities were arguably the result of area biases, in that some of the global wetland models (CLM4Me, IAP-RAS, LPJ-Bern, and LPJ-WHyMe) scaled their intensities to match their global total emissions with those of global inversions, which could result in local biases if their wetland maps suffered from either global or local bias (which was true of these models). Interestingly, several models yielded estimates similar to those of the two regionally optimized UW-VIC simulations, implying that the regional optimization did not confer a distinct advantage on UW-VIC.

Nitrogen limitation influenced intensity in LPX-BERN, the one model that included it. Although we did not plot results from the two LPX-BERN configurations that lacked

nitrogen–carbon interactions in Fig. 5, we compare results from all four LPX-BERN configurations in Table 6. In LPX-BERN (N) and LPX-BERN (DyPTOP-N), the nitrogen limitation imposed by nitrogen–carbon interactions substantially reduced NPP, relative to LPX-BERN and LPX-BERN (DyPTOP), leading to a reduction of mean annual  $\text{CH}_4$  emissions of approximately 20 % over the entire WSL over the period 1993–2010. This reduction was slightly larger than the difference in emissions between simulations using the Sheng2004 map to prescribe peatland area (LPX-BERN and LPX-BERN (N)) and simulations using the DyPTOP method to determine peatland extent dynamically (LPX-BERN (DyPTOP) and LPX-BERN (DyPTOP-N)). In addition, the reduction in emissions due to nitrogen limitation was concentrated in the northern half of the domain, in contrast to the reduction due to dynamic peatland extent, which was concentrated in the southern half of the domain. Nitrogen limitation also reduced trends in  $\text{CH}_4$  emissions over the entire WSL over the period 1993–2010, through reductions in soil carbon accumulation rates. However, both these trends and their reductions were very small ( $< 0.5\%$  per year in most cases) and statistically insignificant over the study period.

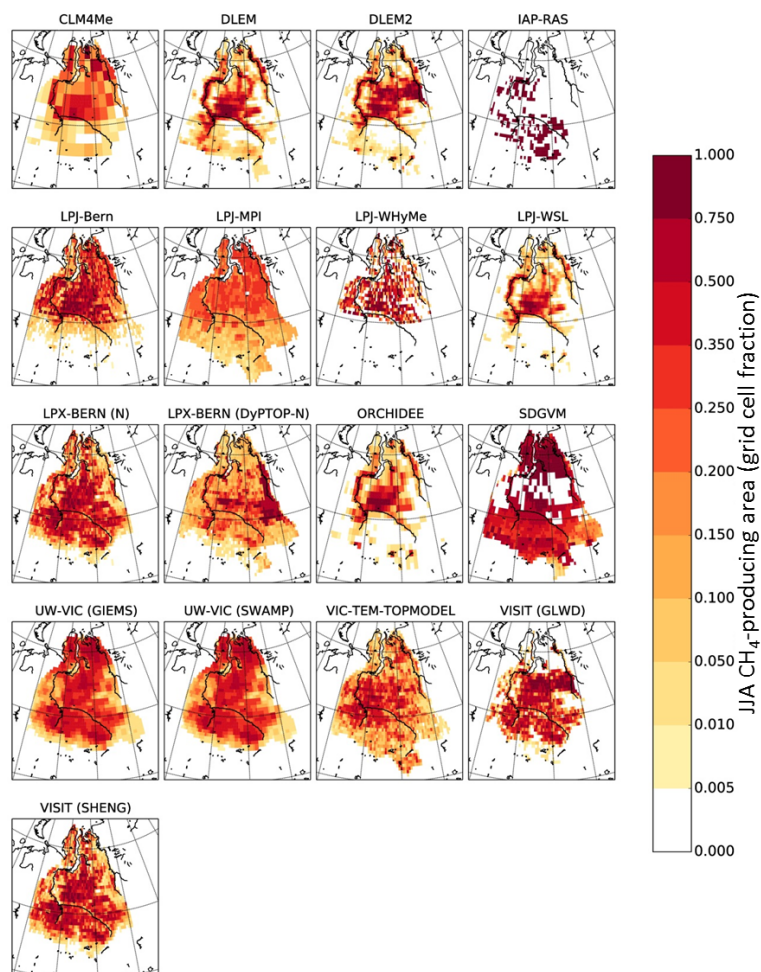


**Figure 7.** Maps of average JJA CH<sub>4</sub>-producing area (fraction of grid cell area) from participating models.

**Table 7.** Temporal coefficients of variation (CV) of annual CH<sub>4</sub> emissions, 1993–2004.

Model	CV	Model	CV	Model	CV
CLM4Me	0.115	LPJ-WSL	0.208	VIC-TEM-TOPMODEL	0.149
DLEM	0.242	LPX-BERN (N)	0.069	VISIT (GLWD)	0.171
DLEM2	0.140	LPX-BERN (DyPTOP-N)	0.076	VISIT (Sheng)	0.163
IAP-RAS	0.091	ORCHIDEE	0.113	Bousquet2011K	0.160
LPJ-Bern	0.087	SDGVM	0.118	Bousquet2011R	0.446
LPJ-MPI	0.195	UW-VIC (GIEMS)	0.338		
LPJ-WHyMe	0.127	UW-VIC (SWAMPS)	0.197		

### 3.4 Model temporal uncertainty and major environmental drivers

#### 3.4.1 Average seasonal cycles

Models demonstrated general agreement on the shape of the seasonal cycle of emissions (Fig. 8, top left) and intensities (Fig. 8, bottom right), despite wide disagreement on the shape and timing of the seasonal cycle of the CH<sub>4</sub>-producing

area (Fig. 8, bottom left). The regional inversions (Kim2011 and Winderlich2012) agreed on a July peak for CH<sub>4</sub>, although Winderlich2012 suggested a noticeably larger contribution from cold season months than the others (which is plausible, given reports of non-zero winter emissions; Rinne et al., 2007; Kim et al., 2007; Panikov and Dedysch, 2000). In contrast, both Bousquet inversions peaked in August. Unlike the other three inversions, the Bousquet2011R inversion had negative emissions (net oxidation) in either May or June



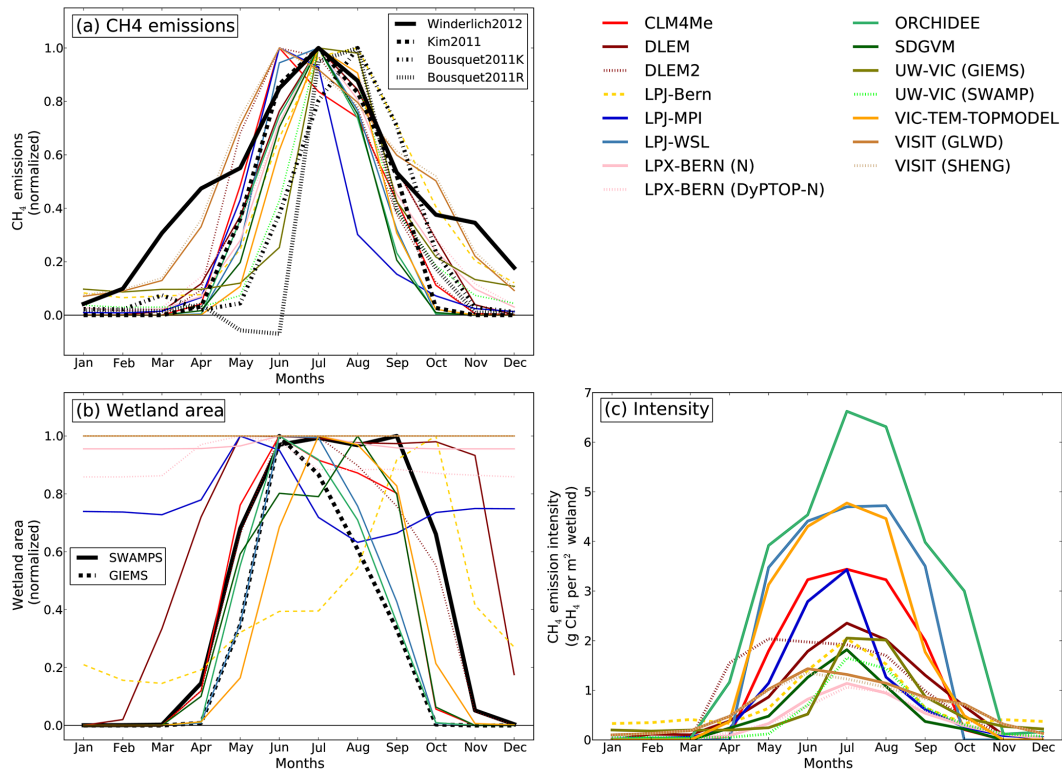


**Figure 8.** Average whole-domain seasonal cycles (1993–2004) of normalized monthly CH<sub>4</sub> emissions (top), normalized monthly CH<sub>4</sub>-producing or surface water areas (lower left), and monthly intensities (g CH<sub>4</sub> m<sup>-2</sup> of wetland area; lower right), with satellite surface water products and inversions for reference. CH<sub>4</sub> emissions and areas have been normalized relative to their peak values.

of almost every year of its record. These negative emissions were widespread, throughout not only the WSL but the entire boreal Asia region, and cast doubt on the accuracy of their seasonal cycle. Turning to the surface water products (Fig. 8, bottom left), GIEMS and SWAMPS displayed quite different shapes in their seasonal cycles of surface water extent: GIEMS exhibited a sharp peak in June and SWAMPS displayed a broad, flat maximum from June through September. In fact, SWAMPS had a similar shape to GIEMS south of about 64° N; the broad peak for the WSL as a whole was the result of late-season peaks further north.

Most models' CH<sub>4</sub> emissions peaked in July, in agreement with the regional inversions. A few models peaked in June: CLM4Me, DLEM2, LPJ-MPI, VISIT (GLWD), and VISIT (Sheng). Correspondingly early peaks in intensity can explain the early peaks in the DLEM2 and the VISIT simulations, indicating either early availability of carbon substrate in the soil or rapid soil warming (the latter is likely for VISIT, given its linearly interpolated soil temperatures). In contrast, LPJ-MPI's early peak in emissions was the result of an early (May) peak in CH<sub>4</sub>-producing area, which, in turn, was the result of early snowmelt. Two models (LPJ-BERN and UW-VIC (GIEMS)) peaked in August. LPJ-Bern's late peak resulted from a late peak in wet mineral soil intensity, despite an exceptionally late (October) peak in CH<sub>4</sub>-producing area.

The late peak of UW-VIC (GIEMS) corresponded to a late peak in intensity, implying either late availability of carbon substrate (due to inhibition of NPP under inundation) or delayed warming of the soil (due to excessive insulation by peat or surface water).

Aside from the above cases, the relative agreement among models on a July peak in CH<sub>4</sub> emissions comes despite wide variation in seasonal cycles of the CH<sub>4</sub>-producing area. For example, DLEM's CH<sub>4</sub>-producing area held steady at its maximum extent from April through November, and VIC-TEM-TOPMODEL's CH<sub>4</sub>-producing area peaked in August, possibly due to low evapotranspiration or runoff rates. Some of the discrepancies in CH<sub>4</sub>-producing area seasonality arose from several models using static maps to define some or all wetland areas (Sects. 2.3 and 2.4). These differences matter little to the seasonal cycle of CH<sub>4</sub> emissions, in part because of the similarity between the seasonal cycles of inundated area and water table depths within the static CH<sub>4</sub>-producing areas and in part because of the nearly universal strong correlation at seasonal timescales between simulated intensities and near-surface air temperature (so that cold-season CH<sub>4</sub>-producing areas have little influence over emissions).

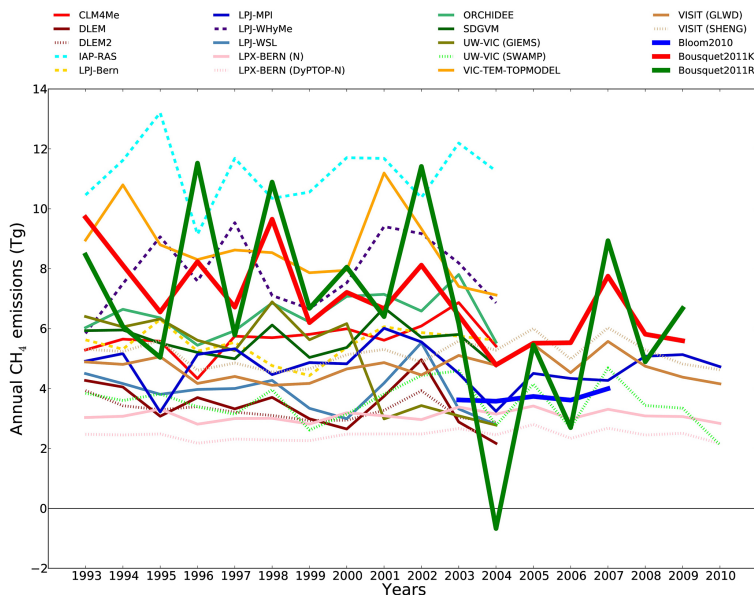


**Figure 9.** Time series of simulated annual total CH<sub>4</sub> emissions (Tg CH<sub>4</sub>) from participating models, the Reference and Kaplan inversions from Bousquet et al. (2011), and the Bloom (2010) inversion.

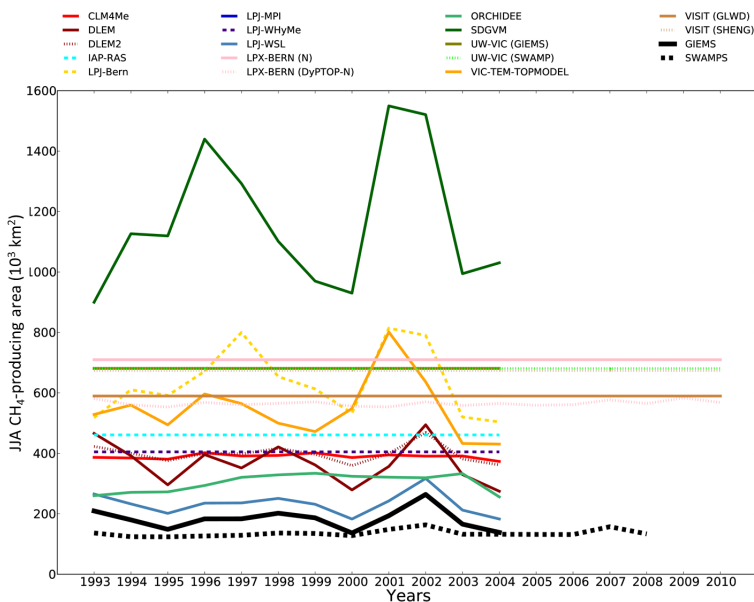


**Figure 10.** Time series of simulated JJA CH<sub>4</sub>-producing areas (10<sup>3</sup> km<sup>2</sup>), with JJA surface water areas from GIEMS and SWAMPS products for reference.

**3.4.2 Interannual variability**

At multiyear timescales (shown for the period 1993–2010 in Fig. 9), models’ and inversions’ total annual CH<sub>4</sub> emissions displayed a wide range of interannual variability, even after accounting for the effects of differences in intensity. Values of the coefficient of variation (CV) for models over the period 1993–2004 ranged from 0.069 (LPX-BERN (N)) to 0.338 (UW-VIC (GIEMS)) with a mean of 0.169 (Ta-

ble 7). While Bousquet2011K’s CV of 0.160 fell near the mean model CV, Bousquet2011R’s CV of 0.446 was 25 % larger than the largest model CV, and over twice the second-largest model CV. Bousquet2011R’s high variability was due in part to a peak in CH<sub>4</sub> emissions in 2002 followed by a large drop in emissions between 2002 and 2004, actually becoming negative (net CH<sub>4</sub> oxidation) in 2004 before continuing at a much lower mean value from 2005 to 2009. This peak and decline coincide with a similar peak and decline in

**Table 8.** Temporal correlations among environmental drivers, 1993–2004.

WSL	CRU T JJA	CRU P JJA	SWAMPS JJA	GIEMS JJA
CRU T JJA	1.00			
CRU P JJA	−0.10	1.00		
SWAMPS JJA	0.14	0.66	1.00	
GIEMS JJA	−0.11	0.44	0.68	1.00
S	CRU T JJA	CRU P JJA	SWAMPS JJA	GIEMS JJA
CRU T JJA	1.00			
CRU P JJA	−0.28	1.00		
SWAMPS JJA	−0.12	0.44	1.00	
GIEMS JJA	−0.10	0.22	0.87	1.00
N	CRU T JJA	CRU P JJA	SWAMPS JJA	GIEMS JJA
CRU T JJA	1.00			
CRU P JJA	−0.06	1.00		
SWAMPS JJA	0.32	0.60	1.00	
GIEMS JJA	−0.05	0.34	0.61	1.00

$F_w$  (Fig. 10) and precipitation (Fig. 11). Several models (notably LPJ-MPI, LPJ-WHyMe, LPJ-WSL, DLEM, and VIC-TEM-TOPMODEL), as well as Bousquet2011K, mirrored this drop to varying degrees, but none dropped as much in proportion to their means or became negative. In contrast, Bloom2010, spanning only the period 2003–2007, exhibited extremely little interannual variability, perhaps due to its use of GRACE as a proxy for inundated area and water table depth.

To investigate the influence of various climate drivers on CH<sub>4</sub> emissions, we computed the individual correlations between the JJA CH<sub>4</sub> emissions and the following JJA drivers: CRU air temperature ( $T_{\text{air}}$ ), CRU precipitation (P), GIEMS  $F_w$ , and SWAMPS  $F_w$ , for forward models and the two Bousquet2011 inversions, over the period 1993–2004 (Table S2). Here we included four additional model configurations that we did not show in previous sections: VISIT (GIEMS-WH), VISIT (SHENG-WH), LPX-BERN, and LPX-BERN-DyPTOP. The two drivers yielding the highest correlations with JJA CH<sub>4</sub> emissions were JJA CRU  $T_{\text{air}}$  and JJA GIEMS  $F_w$ . These two drivers also exhibited nearly zero correlation with each other over the WSL and the south and north halves (Table 8). Because variations in water table position are driven by the same hydrologic factors (snowmelt, rainfall, evapotranspiration, and drainage) that drive variations in  $F_w$ , correlation with  $F_w$  should serve as a general measure of the influence of both surface and sub-surface moisture conditions on methane emissions, even for models that were not explicitly driven by  $F_w$ . Therefore, we chose to examine model behavior in terms of correlations with JJA CRU  $T_{\text{air}}$  and JJA GIEMS  $F_w$ . As an aside, this choice was not an endorsement of GIEMS over SWAMPS (which yielded qualitatively similar results to GIEMS); it simply resulted in better separation among models.

The relative strengths of the correlations between models' CH<sub>4</sub> emissions and drivers varied widely, as shown in the scatterplots in Fig. 12. Over the entire WSL (top left) as well as the south and north halves (bottom left and right), the low correlation between  $T_{\text{air}}$  and  $F_w$  led to consistent trade-offs in the correlations between simulated emissions and  $T_{\text{air}}$  ( $x$  axis) or  $F_w$  ( $y$  axis). Some models (all four LPX-BERN simulations, all four VISIT simulations, IAP-RAS, ORCHIDEE, and SDGVM) had correlations with  $T_{\text{air}}$  that were greater than 0.7 in one or both halves of the domain; since this means that  $T_{\text{air}}$  would explain the majority of CH<sub>4</sub> variance in a linear model, we have denoted them as “ $T_{\text{air}}$ -dominated”. Other models (DLEM, LPJ-WSL, DLEM2, and LPJ-MPI) were “ $F_w$ -dominated” in one or both halves of the domain. For the other models and inversions, no driver explained the majority of the variance. A few models had small enough contributions from one or the other driver for the resulting correlations to be negative, due to the small negative correlation between  $T_{\text{air}}$  and  $F_w$ . Neither of the two Bousquet2011 inversions exhibited strong correlations with either  $F_w$  or  $T_{\text{air}}$ , which might imply that models also should not exhibit strong correlations with one driver.

Indeed, the overarching pattern in the model correlations was that models that lacked physical and biochemical formulations appropriate to the high latitudes exhibited stronger correlations with inundation or air temperature than either the inversions or more sophisticated models. One characteristic that most of the  $F_w$ -dominated models (except for DLEM2) have in common is that they lack soil thermal formulations that account for soil freeze–thaw processes; conversely, most of the non- $F_w$ -dominated models do have such formulations. In addition, inundated fractions of DLEM, DLEM2, and LPJ-WSL were explicitly driven by GIEMS  $F_w$ . Unlike the other three models, LPJ-MPI does account for the thermal effects

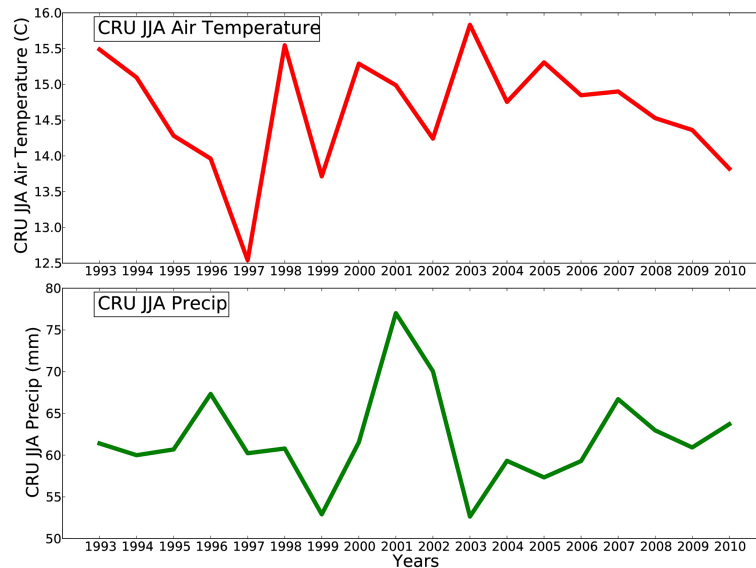


**Figure 11.** Time series of CRU JJA air temperature (°C) and precipitation (mm).

of peat soils, which might explain LPJ-MPI's low (slightly negative) correlation with air temperature.

Some of the  $T_{\text{air}}$ -dominated models also lack sophisticated soil thermal physics. VISIT's strong correlation with  $T_{\text{air}}$  can be explained by the fact that its soil temperature scheme is a simple linear interpolation between current air temperature at the surface and annual average air temperature at the bottom of the soil column; as a result, VISIT's soil temperature has a 1.0 correlation with air temperature. Comparing the WH configurations of VISIT to the default configurations, the model of Walter and Heimann (2000) had a lower correlation with air temperature than the Cao (1996) model. SDGVM also lacks soil freeze–thaw dynamics. IAP-RAS assumes all wetlands are completely saturated and holds their areas constant in time; as a result, its  $\text{CH}_4$  emissions have no dependence on soil moisture or  $F_w$  but a strong dependence on air temperature. LPX-BERN's high correlation with air temperature is the result of a relative insensitivity of  $\text{CH}_4$  emissions to water table depth, but at present there are too few sites with multi-year observations in the region to determine whether this low sensitivity is reasonable. Nitrogen–carbon interaction (LPX-BERN (N) and LPX-BERN (DyPTOP-N)) appeared to have only a minor effect on LPX-BERN's interannual variability in the north but led to a slight reduction in correlation with  $T_{\text{air}}$  in the south. Finally, UW-VIC (GIEMS) had small negative correlations with both  $T_{\text{air}}$  and  $F_w$  in the north, likely the result of its surface water formulation. UW-VIC's surface water dynamics had been initially calibrated using the SWAMPS product; the much larger surface water extents of GIEMS in the north resulted in substantially deeper surface water, with corresponding insulating effects, greater evaporative cooling, and longer residence times, thus lowering correlations with both observed  $F_w$  and  $T_{\text{air}}$ . The large differ-

ence in behavior between UW-VIC (GIEMS) and UW-VIC (SWAMPS) implies that the differences arising from optimizing surface water dynamics to different products far outweighed the differences between UW-VIC and other models in their selection of biogeochemical parameters.

## 4 Discussion

### 4.1 Long-term means and spatial distributions

The most striking finding, in terms of long-term means and spatial distributions, was the substantial bias in  $\text{CH}_4$  emissions that resulted from using satellite surface water products or inaccurate wetland maps to delineate wetlands. Surface water is an important component of wetland models, but it clearly is a poor proxy for wetland extent at high latitudes because it both excludes the large expanses of strongly emitting non-inundated peatlands that exist there (Sect. 2.1) that were missed by GIEMS and underrepresented by SWAMPS and erroneously includes the high concentrations of large lakes there (e.g., Lehner and Döll, 2004), which do not necessarily emit methane at the same rates or via the same carbon cycling processes as wetlands (e.g., Walter et al., 2006; Pace et al., 2004). The practical difficulties in detecting inundation under forest canopies with visible or high-frequency microwave sensors (e.g., Sippel and Hamilton, 1994) compound these problems. In the case of the WSL, equating wetlands with surface water not only caused underestimation of total  $\text{CH}_4$  emissions but also led to the attribution of the majority of the region's emissions to the permafrost zone in the north. This issue is not unique to the WSL, as the collocation of permafrost, lakes, and inundation is present throughout the high latitudes (Tarnocai et al., 2009; Lehner

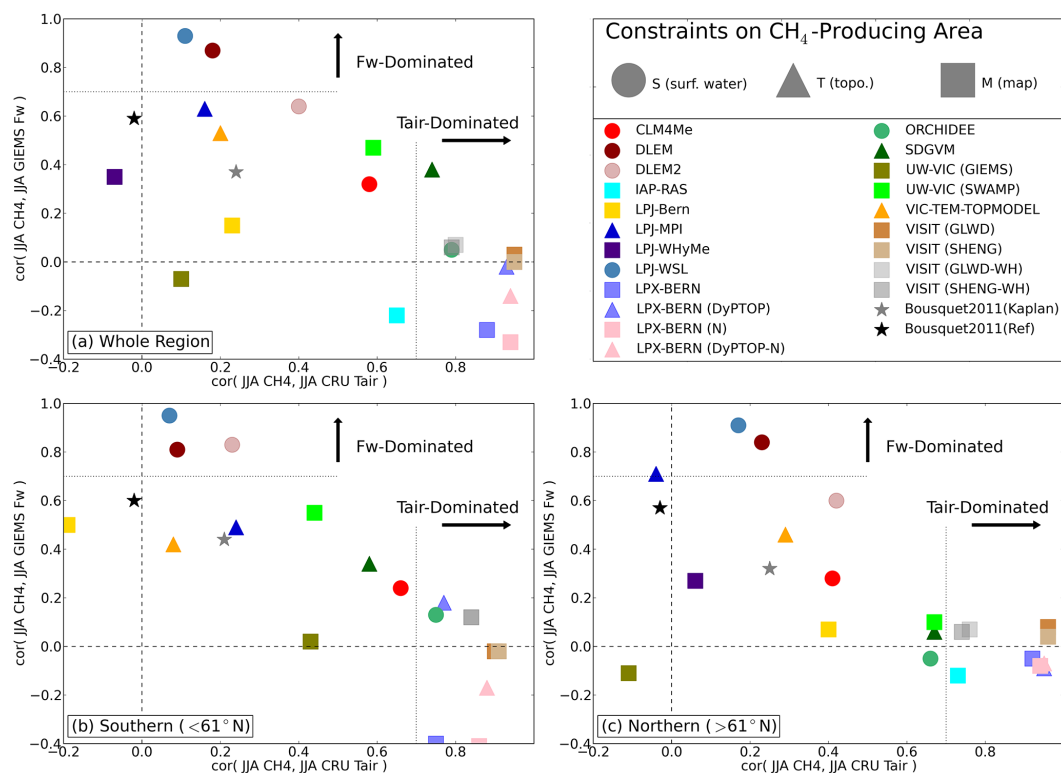


**Figure 12.** Influence of interannual variations in surface water area fraction ( $F_w$ ) on model  $\text{CH}_4$  emissions (expressed as correlation between JJA GIEMS  $F_w$  and JJA  $\text{CH}_4$ ) vs. influence of air temperature ( $T_{\text{air}}$ ) on model  $\text{CH}_4$  emissions (expressed as correlation between JJA CRU  $T_{\text{air}}$  and JJA  $\text{CH}_4$ ), for the entire WSL (top) and the southern and northern halves of the domain (bottom).  $F_w$ -Dominated and  $T_{\text{air}}$ -Dominated denote correlation thresholds above which surface water area or air temperature, respectively, explain more than 50 % of the variance in  $\text{CH}_4$  emissions. Circles denote models that used satellite surface water products alone (corresponding to code S in Table 2) to delineate wetlands. Triangles denote models that used topographic information, with or without surface water products (corresponding to code T in Table 2). Squares denote models that used wetland maps with or without topography or surface water products (corresponding to code M in Table 2).

and Döll, 2004; Brown et al., 1998). Indeed, in their analysis of the Hudson Bay Lowland (HBL), Melton et al. (2013) found that three of the four lowest emissions estimates were from S models (CLM4Me, DLEM, and LPJ-WSL), although whether this was due to a bias in area was not examined. Given present concerns over the potential liberation of labile carbon from thawing permafrost over the next century (Koven et al., 2011), it is crucial to avoid under- or overestimating emissions from permafrost wetlands.

It is therefore important for modelers – both forward and inverse – to use accurate wetland maps such as Pregon et al. (2008), Sheng et al. (2004), or Lehner and Döll (2004) in their model development, whether as a static input parameter or as a reference for evaluating prognostically computed  $\text{CH}_4$ -producing areas, and to account for the existence of non-inundated portions within these wetlands in which methane emissions have a dependence on water table depth. Maps such as Tarnocai et al. (2009) may be inappropriate unless restricting simulations to permafrost wetlands. Ideally, modelers would be able to draw on a global version of the high-resolution map of Pregon et al. (2008) that not only de-

lineates wetlands but also identifies the major subtypes (e.g., sphagnum-dominated or sedge-dominated, as in Lupascu et al., 2012) to which different methane emissions parameters could potentially be applied. When using surface water products to constrain simulated inundated extents, modelers must be sure either to mask out permanent lakes and large rivers, using a data set such as GLWD (Lehner and Döll, 2004) or MOD44W (Carroll et al., 2009), or better, to implement carbon cycling processes that are appropriate to these forms of surface water.

#### 4.2 Temporal variability, environmental drivers, and model features

Another notable finding was that models that lacked physical and biochemical formulations appropriate to the high latitudes exhibited more extreme correlations with  $F_w$  or air temperature than either inversions or more sophisticated models. In other words, high-latitude biogeophysical processes – specifically, soil freeze–thaw, the insulating effects of snow and peat, and relationships between emissions and water table depth in peatlands – make a substantial difference

to the sensitivities of emissions to environmental drivers, at least over the 12-year period of this study. Even if we do not fully trust the Bousquet2011 inversions, it seems reasonable to assume that the models that simulate high-latitude-specific processes are more likely to be correct in this regard than the other models. These sensitivities have a bearing on models' responses to potential future climate change (e.g., Riley et al., 2011; Koven et al., 2011).

Thus, it appears that the following model features are desirable for reliable simulations of boreal wetlands:

- realistic soil thermal physics, including freeze–thaw dynamics. Most of the models that were highly correlated with one driver (LPJ-WSL, DLEM, LPJ-MPI, VISIT, and SDGVM) lacked this feature.
- accurate representations of peat soils. Again, many of the models with high correlations with one driver (LPJ-WSL, DLEM, VISIT, and SDGVM) lacked this feature.
- realistic representations of unsaturated (non-inundated) peatlands, including the dependence of CH<sub>4</sub> emissions on water table depth. LPJ-WSL, an  $F_w$ -dominated model, effectively set non-inundated CH<sub>4</sub> emissions to 0 because it did not simulate wetlands outside of the time-varying GIEMS surface water area. At the other extreme, IAP-RAS, a  $T_{\text{air}}$ -dominated model, treated all wetlands in their static map as if they were saturated, thereby eliminating the contribution of soil moisture variability. The relative insensitivity of LPX-BERN's emissions to water table position similarly reduced the contribution of soil moisture variability, although there are too few observations to say whether this is unreasonable.

Other model features either made relatively little difference in this study or were severely underrepresented but warrant further investigation. This is especially true of biogeochemical processes. For example, whether models contained dynamic vegetation (phenology and/or community composition) or dynamic peatland (peat accumulation and loss) components did not affect performance. However, our 12-year study period was likely too short to see the effects of these features. Changes in vegetation community composition may become more important in end-of-century projections (e.g., Alo and Wang, 2008; Kaplan and New, 2006). In particular, recent studies (Koven et al., 2011; Ringeval et al., 2011; Riley et al., 2011) have found a “wetland feedback”, in which vegetation growth in response to future climate change can lower water tables and reduce inundated extents via increased evapotranspiration. This drying effect reduces end-of-century CH<sub>4</sub> emissions from an approximate doubling of current rates without the feedback to only a 20–30 % increase with the feedback. Similarly, hydrologic and chemical changes in peat soils, in response to disturbances such as permafrost thaw or drainage for mining or agricul-

tural purposes, may be important in end-of-century projections (e.g., Strack et al., 2004). However, to properly assess the accuracy of dynamic vegetation or peatland schemes and their effects on CH<sub>4</sub> emissions, a longer historical study period, along with longer observational records (including observations of species compositions and soil carbon densities) would be necessary.

Other features may warrant further study. Replacing the Cao (1996) model with the model of Walter and Heimann (2000) modestly lowered VISIT's otherwise extreme correlation with  $T_{\text{air}}$ . It is not clear if this is an inherent difference between the two formulations or just an artifact of their parameter values in VISIT, but it might imply that the Walter and Heimann model is more appropriate for applications at high latitudes. Similarly, nitrogen–carbon interaction had a substantial latitude-dependent effect on mean CH<sub>4</sub> emissions for LPX-BERN (Table 6). Again, the size of the effect could be model-dependent, and potential impacts on sensitivities to climate change might become more apparent over a longer analysis period.

Some of the scatter in model sensitivities to drivers may come from differences in the values of parameters related to methane production, methane oxidation, and plant-aided transport, which recent studies (Riley et al., 2011; Berrittella and van Huissteden, 2011) have found to be particularly influential over wetland CH<sub>4</sub> emissions. The investigation of these parameters over the WSL in a model intercomparison can be difficult due to the many large differences among model formulations. As shown in Sects. 3.3 and 3.4.2, the methods of biogeochemical parameter selection had far less influence over the model results than the presence or absence of major features such as sophisticated soil thermal physics. Such a comparison would require the examination of a subset of the models that have sufficiently similar snow, soil, and water table formulations in order to isolate the effects of microbial and vegetative parameters.

Other features that were not investigated here could have potentially large impacts on the response of high-latitude wetlands to future climate change. One such feature is acclimatization, in which soil microbial communities gradually adapt to the long-term mean soil temperature. This feature has been explored in the ORCHIDEE model (Koven et al., 2011; Ringeval et al., 2010), where it greatly reduced the response of wetland CH<sub>4</sub> emissions to long-term temperature changes. Unfortunately, the version of ORCHIDEE used in this study and in the original WETCHIMP study (Melton et al., 2013; Wania et al., 2013) did not use acclimatization. Acclimatization likely would lower ORCHIDEE's correlation with  $T_{\text{air}}$  over timescales long enough for changes in the long-term mean to be as large as interannual anomalies. Another feature explored by Koven et al. (2011) is the liberation of ancient labile carbon stored in permafrost. As with dynamic vegetation, a robust evaluation of these effects would require a much longer study period.

### 4.3 Future needs for observations and inversions

The wide disagreement among estimates from observations and inversions hampers our ability to assess model performance. Given the large influence that wetland maps can have on emissions estimates (not only in the WSL, but over larger areas, as shown by Petrescu et al., 2010), care must be taken to select appropriate maps. Ideally, global satellite or map products such as the GLWD (which omitted the northernmost wetlands in the WSL) should be validated against more intensively ground-truthed regional maps, such as Sheng2004 and Peregon2008, where such maps exist. Similarly, resolving the discrepancies between the GIEMS and SWAMPS remote-sensing surface water products would require verification against independent observations.

The large discrepancy between the spatial distributions of emissions from Glagolev2011 and Kim2011 (concentrated in the south) and Winderlich2012 and Bousquet2011K (concentrated in the north) may be due to several factors. First, the inversions' posterior estimates reflect their prior distributions: Kim2011 used an earlier version of Glagolev2011 (Glagolev et al., 2010) as its prior, while Winderlich2012 and Bousquet2011K both used the Kaplan (2002) distribution as their prior. Second, different types and locations of observations were used: Glagolev2011 was based on in situ chamber measurements of CH<sub>4</sub> fluxes, 80 % of which were obtained south of the Ob' River, while Winderlich2012 was based on atmospheric CH<sub>4</sub> concentrations observed at towers near or north of the Ob' River. Third, observations were not taken from the same years. Finally, the Winderlich2012 wetland CH<sub>4</sub> emissions may have been influenced by assumed emission rates from fossil fuel extraction and biomass burning, which were not adjusted during the inversion. Efforts like the revision of Glagolev2011 will certainly help in resolving some discrepancies, but all estimates would benefit from incorporating observations over long time periods and wider areas to reduce uncertainties in their long-term means.

The global inversions were also subject to uncertainties. For example, while the Bousquet2011 inversions imply that wetland CH<sub>4</sub> emissions in the WSL are not strongly correlated with either  $F_w$  or air temperature, the Bousquet2011 inversions' temporal behaviors must be evaluated with caution. The reference inversion's coefficient of variability (CV), which resulted in net negative annual emissions over the WSL in 2004, was substantially higher than the highest model CV. Bousquet et al. (2006) noted that their inversions were more sensitive to the interannual variability of wetland emissions than to their mean; accordingly, it is possible that the Bousquet2011 inversions underestimated the long-term mean, thereby raising the CV. Another possibility is that the monthly coefficients that optimized total emissions over all of boreal Asia were not optimal over the WSL alone, since the environmental drivers interacting with wetlands elsewhere may not have been in phase with those in the WSL. A further possibility, given credence by the ref-

erence inversion's consistent net negative emissions over all of boreal Asia in May and June, is that errors in other components of the inversion (e.g., atmospheric OH concentrations, methane oxidation rates, background methane concentrations advected from elsewhere) influenced wetland emissions. Finally, other methane sources that were not accounted for in the inversion might have been attributed to wetlands, for example, geological CH<sub>4</sub> seeps (Etiope et al., 2008), leaks from gas pipelines (Ulmishek, 2003), or lakes (Walter et al., 2006).

At the other extreme, the Bloom2010 product exhibited almost no spatial or temporal variability. This might be an artifact of using GRACE data as a proxy for wetland inundation and water table levels. The spatiotemporal accuracy of Bloom2010 must also be questioned, given that it did not use an atmospheric transport model or account for methane oxidation in the atmosphere. Thus, while Bloom2010 provided a useful estimate of long-term mean emissions, it was less helpful in constraining model responses to climate drivers.

Another general limitation of inversions and observations, distinct from estimates of long-term mean emissions, is the lack of sufficiently long periods of record to assess model sensitivities to environmental drivers and climate change. The Bousquet2011 inversions and the SWAMPS surface water product are long enough to begin to address this issue on the global scale, but the Bousquet2011 inversions are not optimized for the WSL. Regional inversions such as Kim2011 and Winderlich2012, which might offer more spatially accurate estimates for the WSL than the Bousquet2011 inversions, only offer a single year of posterior emissions. Long records of in situ observations of CH<sub>4</sub> emissions and the factors that most directly influence these emissions (e.g., soil temperature and water table depth) only exist in a handful of locations (e.g., the Bakchar Bog in the WSL; Panikov and Dedysh, 2000; Friborg et al., 2003; Glagolev et al., 2011). Indeed, the paucity of long in situ records limited our ability to evaluate LPX-BERN's relatively low sensitivity to water table depth. Year-round observations would also be helpful, as winter emissions are sparsely sampled (Rinne et al., 2007; Kim et al., 2007; Panikov and Dedysh, 2000) and inversions disagree as to the magnitude of winter emissions (Fig. 8). The recent implementation of tower networks in the WSL (Sasakawa et al., 2010; Winderlich et al., 2010) show some promise in this regard, as their observations are both multiyear and year-round. More comprehensive observations of emissions from non-wetland methane sources such as seeps, pipe leaks, and lakes, most of which have so far not been accounted for in inversions (although pipe leaks are now being considered; Berchet et al., 2014), would be beneficial in increasing the accuracy of inversions.

## 5 Conclusions

We compared CH<sub>4</sub> emissions from 21 large-scale wetland models, including the models from the WETCHIMP project, to 5 inversions and several observational data sets of CH<sub>4</sub> emissions, surface water area, and total CH<sub>4</sub>-producing area over the West Siberian Lowland (WSL) over the period 1993–2004. Despite the large scatter of individual estimates, mean estimates of annual total emissions over the WSL from forward models ( $5.34 \pm 0.54$  Tg CH<sub>4</sub> yr<sup>-1</sup>), inversions ( $6.06 \pm 1.22$  Tg CH<sub>4</sub> yr<sup>-1</sup>), and observations ( $3.91 \pm 1.29$  Tg CH<sub>4</sub> yr<sup>-1</sup>) largely agreed. However, it was clear that reliance on satellite surface water products alone to delineate wetlands caused substantial biases in long-term mean CH<sub>4</sub> emissions over the region. Models and inversions largely agreed on the timing of the seasonal cycle of emissions over the WSL, but some outliers in the timing of peaks in the simulated inundated area indicated potential inaccuracies in simulating the timing of snowmelt and drainage rates. Models and inversions also displayed a wide range of interannual variability: the CV of the Bousquet2011 reference inversion was more than twice the CVs of all but one model, while the CV of the Bloom2010 inversion was essentially 0. Summer CH<sub>4</sub> emissions from the Bousquet2011 inversions exhibited only weak correlations with summer air temperature or inundation. Models that accounted for soil thermal physics and realistic methane–soil moisture relationships similarly tended to have low to moderate correlations with both inundation and air temperature, due in part to the competing influences of temperature and moisture, and in part to the insulating effects of snow and peat soils. In contrast, models lacking these formulations tended to be either inundation- or temperature-dominated (either inundation or temperature accounted for more than 50 % of the variance).

Based on our findings, we have the following recommendations for simulating CH<sub>4</sub> emissions from high-latitude wetlands:

- Forward and inverse models should use the best available wetland maps, either as inputs or as targets for optimization of dynamic wetland schemes. Satellite-derived surface water products are a poor proxy for wetland extent, due to (a) misclassifying large areas of high-latitude peatlands that can emit methane when the water table is below the surface; (b) often including permanent water bodies, whose carbon cycling dynamics can be substantially different from those of wetlands; and (c) difficulties in detecting inundation under forest canopies. To improve the accuracy of global wetland map products may require combining information from satellite products and canonical maps.
- Models must account for emissions from non-inundated wetlands, with realistic relationships between emissions and water table depth.
- Models should implement realistic soil thermal physics and snow schemes and account for the presence of peat soils at high latitudes.
- Multiyear and multidecade observational and inversion products are crucial for assessing whether model simulations capture the correct sensitivities of wetland CH<sub>4</sub> emissions to environmental drivers.

**The Supplement related to this article is available online at doi:10.5194/bg-12-3321-2015-supplement.**

*Author contributions.* T. J. Bohn and J. R. Melton jointly conceived and designed this study with input from J. O. Kaplan. J. R. Melton provided the results from the original WETCHIMP models. T. J. Bohn, A. Ito, T. Kleinen, R. Spahni, B. D. Stocker, B. Zhang, and X. Zhu provided results for the other non-WETCHIMP models. R. Schroeder and K. C. McDonald provided the SWAMPS data set. M. V. Glagolev provided the Glagolev et al. (2011) data set and information on fossil methane seeps. S. Maksyutov provided the Kim et al. (2011) inversion and the Peregon et al. (2008) wetland map. V. Brovkin provided the Winderlich (2012) inversion. T. J. Bohn processed and reformatted results of all models, observations, and inversions and analyzed the results. T. J. Bohn and J. R. Melton collaborated on all figures. T. J. Bohn prepared the manuscript with contributions from all coauthors.

*Acknowledgements.* The WETCHIMP project received support for collaboration from the COST Action TERRABITES (ES0804). We thank Dennis P. Lettenmaier at the University of Washington and NASA grant NNX11AR16G from the Northern Eurasian Earth Science Partnership Initiative (NEESPI) for the use of computational resources. T. J. Bohn was supported by grant 1216037 from the US National Science Foundation (NSF) Science, Engineering and Education for Sustainability (SEES) Post-Doctoral Fellowship program. J. R. Melton was supported by a National Science and Engineering Research Council of Canada (NSERC) visiting Post-Doctoral Fellowship. T. Kleinen was supported by the German Ministry of Education and Research (CarboPerm-Project, BMBF Grant No. 03G0836C). R. Spahni was supported by the Swiss National Science Foundation and by the European Commission through the FP7 project Past4Future (grant No. 243908). B. D. Stocker was supported by ERC FP7 project EMBRACE (grant No. 282672). H. Tian and B. Zhang were supported by US National Science Foundation (EaSM: AGS-1243220). Q. Zhuang and X. Zhu were supported by the US Department of Energy with project No. DE-SC0007007. M. V. Glagolev was supported by a grant in accordance with the Tomsk State University Competitiveness Improvement Program. S. Maksyutov was supported by Grant A-1202 of Environment Research and Technology Development Fund (ERTDF), Ministry of Environment Japan. S. N. Denisov and A. V. Eliseev were supported by the Russian President grant NSh-3894.2014.5 and by the Russian Foundation for Basic Research grant 15-05-02457. A. Gallego-Sala was supported by a Natural



Environment Research Council grant (NERC Standard grant NE/I012915/1). W. J. Riley and Z. M. Subin were supported by the US Department of Energy contract No. DE-AC02-05CH11231 under the Regional and Global Climate Modeling (RGCM) Program and the Next-Generation Ecosystem Experiments (NGEE Arctic) project. We thank Ben Poulter, at Montana State University, and Elke Hodson, at the US Department of Energy, for the results of LPJ-WSL. We thank Rita Wania for the results of LPJ-WhyMe. We thank Bruno Ringeval, at the Institut National de la Recherche Agronomique, France, for the results of ORCHIDEE. We thank Peter Hopcroft and Joy Singarayer, at University of Bristol, UK, for the results of SDGVM. We thank A. Anthony Bloom, at the University of Edinburgh, UK, for the Bloom et al. (2010) inversion. We thank Philippe Bousquet, at the Laboratoire des Sciences du Climat et de l'Environnement, France, for the Reference and Kaplan inversions from Bousquet et al. (2011). We thank Catherine Prigent, at the Observatoire de Paris, France, and Fabrice Papa, at the Laboratoire d'Études en Géophysique et Océanographie Spatiales, France, for the GIEMS data set. We thank Laurence Smith at the University of California, Los Angeles, for the Sheng et al. (2004) data set. We thank Anna Peregón, at Laboratoire des Sciences du Climat et de l'Environnement, France, for the Peregón et al. (2008) data set. We thank Elaine Matthews, at NASA/Goddard Institute for Space Studies, for valuable feedback.

Edited by: P. Stoy

## References

- Alo, C. A. and Wang, G.: Potential future changes of the terrestrial ecosystem based on climate projections by eight general circulation models, *J. Geophys. Res.-Biogeophys.*, 113, G01004, doi:10.1029/2007JG000528, 2008.
- Amante, C. and Eakins, B. W.: ETOPO1 1 Arc-Minute Global Relief Model: Procedures, Data Sources and Analysis, NOAA Technical Memorandum NESDIS NGDC-24, National Geophysical Data Center, NOAA, doi:10.7289/V5C8276M (last access: April 2013), 2009.
- Berchet, A., Pison, I., Chevallier, F., Paris, J.-D., Bousquet, P., Bonne, J.-L., Arshinov, M. Y., Belan, B. D., Cressot, C., Davydov, D. K., Dlugokencky, E. J., Fofonov, A. V., Galanin, A., Lavric, J., Machida, T., Parker, R., Sasakawa, M., Spahni, R., Stocker, B. D., and Winderlich, J.: Natural and anthropogenic methane fluxes in Eurasia: a meso-scale quantification by generalized atmospheric inversion, *Biogeosciences Discuss.*, 11, 14587–14637, doi:10.5194/bgd-11-14587-2014, 2014.
- Berrittella, C. and van Huissteden, J.: Uncertainties in modeling CH<sub>4</sub> emissions from northern wetlands in glacial climates: the role of vegetation parameters, *Clim. Past*, 7, 1075–1087, doi:10.5194/cp-7-1075-2011, 2011.
- Beven, K. J. and Kirkby, M. J.: A physically based, variable contributing area model of basin hydrology, *Hydrol. Sci. Bull.*, 24, 43–69, 1979.
- Bloom, A. A., Palmer, P. I., Fraser, A., Reay, D. S., and Frankenberg, C.: Large-Scale Controls of Methanogenesis Inferred from Methane and Gravity Spaceborne Data, *Science*, 327, 322–325, doi:10.1126/science.1175176, 2010.
- Bohn, T. J., Lettenmaier, D. P., Sathulur, K., Bowling, L. C., Podest, E., McDonald, K. C., and Friborg, T.: Methane emissions from western Siberian wetlands: heterogeneity and sensitivity to climate change, *Environ. Res. Lett.*, 2, 045015, doi:10.1088/1748-9326/2/4/045015, 2007.
- Bohn, T. J., Podest, E., Schroeder, R., Pinto, N., McDonald, K. C., Glagolev, M., Filippov, I., Maksyutov, S., Heimann, M., Chen, X., and Lettenmaier, D. P.: Modeling the large-scale effects of surface moisture heterogeneity on wetland carbon fluxes in the West Siberian Lowland, *Biogeosciences*, 10, 6559–6576, doi:10.5194/bg-10-6559-2013, 2013.
- Bousquet, P., Ciais, P., Miller, J. B., Dlugokencky, E. J., Hauglustaine, D. A., Prigent, C., Van der Werf, G. R., Peylin, P., Brunke, E.-G., Carouge, C., Langenfelds, R. L., Lathière, J., Papa, F., Ramonet, M., Schmidt, M., Steele, L. P., Tyler, S. C., and White, J.: Contribution of anthropogenic and natural sources to atmospheric methane variability, *Nature*, 443, 439–443, doi:10.1038/nature05132, 2006.
- Bousquet, P., Ringeval, B., Pison, I., Dlugokencky, E. J., Brunke, E.-G., Carouge, C., Chevallier, F., Fortems-Cheiney, A., Frankenberg, C., Hauglustaine, D. A., Krummel, P. B., Langenfelds, R. L., Ramonet, M., Schmidt, M., Steele, L. P., Szopa, S., Yver, C., Viovy, N., and Ciais, P.: Source attribution of the changes in atmospheric methane for 2006–2008, *Atmos. Chem. Phys.*, 11, 3689–3700, doi:10.5194/acp-11-3689-2011, 2011.
- Bovensmann, H., Burrows, J. P., Buchwitz, M., Frerick, J., Noël, S., Rozanov, V. V., Chance, K. V., and Goede, A. P. H.: SCIAMACHY: Mission objectives and measurement modes, *J. Atmos. Sci.*, 56, 127–150, 1999.
- Brown, J., Ferrians Jr., O. J., Heginbottom, J. A., and Melnikov, E. S.: Circum-Arctic map of permafrost and ground-ice conditions, Boulder, CO: National Snow and Ice Data Center/World Data Center for Glaciology, Digital media, [http://nsidc.org/data/docs/fgdc/ggd318\\_map\\_circumarctic/](http://nsidc.org/data/docs/fgdc/ggd318_map_circumarctic/) (last access: 20 May 2015), 1998.
- Cao, M. K., Marshall, S., and Gregson, K.: Global carbon exchange and methane emissions from natural wetlands: Application of a process-based model, *J. Geophys. Res.-Atmos.*, 101, 14399–14414, 1996.
- Carroll, M. L., Townshend, J. R., DiMiceli, C. M., Noojipady, P., and Sohlberg, R. A.: A new global raster water mask at 250 m resolution, *Int. J. Digital Earth*, 2, 291–308, 2009.
- Christensen, T. R., Ekberg, A., Strom, L., Mastepanov, M., Panikov, N., Öquist, M., Svensson, B. H., Martikainen, P. J., and Oskarsson, H.: Factors controlling large scale variations in methane emissions from wetlands, *Geophys. Res. Lett.*, 30, 1414, doi:10.1029/2002GL016848, 2003.
- Christensen, T. R., Johansson, R. T., Akerman, H. J., Mastepanov, M., Malmer, N., Friborg, T., Crill, P., and Svensson, B. H.: Thawing sub-arctic permafrost: Effects on vegetation and methane emissions, *Geophys. Res. Lett.*, 31, L04501, doi:10.1029/2003GL018680, 2004.
- Clymo, R. S., Kramer, J. R., and Hammerton, D.: Sphagnum-dominated peat bog: a naturally acid ecosystem [and discussion], *Philos. T. R. Soc. Lond. B*, 305, 487–499, 1984.
- Dorrepaal, E., Toet, S., van Logtestijn, R. S., Swart, E., van de Weg, M. J., Callaghan, T. V., and Aerts, R.: Carbon respiration from subsurface peat accelerated by climate warming in the subarctic, *Nature*, 460, 616–619, 2009.
- Efremova, T. T., Sekretenko, O. P., Avrova, A. F., and Efremov, S. P.: Spatial structure of acid properties of litter in the suc-

- cession row of swamp birch woods, *Biol. Bull.*, 41, 284–295, doi:10.1134/S106235901305004X, 2014.
- Eliseev, A. V., Mokhov, I. I., Arzhanov, M. M., Demchenko, P. F., and Denisov, S. N.: Interaction of the methane cycle and processes in wetland ecosystems in a climate model of intermediate complexity, *Izv. Atmos. Ocean. Phys.*, 44, 139–152, 2008.
- Eppinga, M. B., Rietkerk, M., Borren, W., Lapshina, E. D., Bleuten, W., and Wassen, M. J.: Regular surface patterning of peatlands: Confronting theory with field data, *Ecosystems*, 11, 520–536, 2008.
- Etiopie, G., Lassey, K. R., Klusman, R. W., and Boschi, E.: Reappraisal of the fossil methane budget and related emission from geologic sources, *Geophys. Res. Lett.*, 35, L09307, doi:10.1029/2008GL033623, 2008.
- ETOPO: 2-minute gridded global relief data (ETOPO2v2), US Department of Commerce, National Oceanic and Atmospheric Administration, National Geophysical Data Center, available at: <http://www.ngdc.noaa.gov/mgg/fliers/06mgg01.html> (last access: 14 August 2012), 2006.
- Farr, T. G., Rosen, P. A., Caro, E., Crippen, R., Duren, R., Hensley, S., Kobrick, M., Paller, M., Rodriguez, E., Roth, L., Seal, D., Shaffer, S., Shimada, J., Umland, J., Werner, M., Oskin, M., Burbank, D., and Alsdorf, D.: The shuttle radar topography mission, *Rev. Geophys.*, 45, RG2004, doi:10.1029/2005RG000183, 2007.
- Friberg, T., Soegaard, H., Christensen, T. R., and Panikov, N. S.: Siberian wetlands: Where a sink is a source, *Geophys. Res. Lett.*, 30, 2129, doi:10.1029/2003GL017797, 2003.
- Fridland, V. M.: Pochvennaya karta RSFSR (Soil map of the RSFSR), scale 1 : 2500 000, V. V. Dokuchayev Soils Inst., Admin. for Geod. and Cartogr., Gosagroprom, Moscow, 1988.
- Friedl, M. A., Sulla-Menashe, D., Tan, B., Schneider, A., Ramankutty, N., Sibley, A., and Huang, X.: MODIS Collection 5 global land cover: Algorithm refinements and characterization of new datasets, *Remote Sens. Environ.*, 114, 168–182, 2010.
- Frolking, S., Roulet, N., and Lawrence, D.: Issues related to incorporating northern peatlands in to global climate models, *Carbon Cycling in Northern Peatlands*, edited by: Baird, A. J., Belyea, L. R., Comas, X., Reeve, A. S., and Slater, L. D., 19–35, 2009.
- Frolking, S., Talbot, J., Jones, M. C., Treat, C. C., Kauffman, J. B., Tuittila, E. S., and Roulet, N.: Peatlands in the Earth's 21st century climate system, *Environ. Rev.*, 19, 371–396, 2011.
- Fung, I., John, J., Lerner, J., Matthews, E., Prather, M., Steele, L. P., and Fraser, P. J.: Three-dimensional model synthesis of the global methane cycle, *J. Geophys. Res.-Atmos.*, 96, 13033–13065, 1991.
- Gedney, N., Cox, P. M., and Huntingford, C.: Climate feedback from wetland methane emissions, *Geophys. Res. Lett.*, 31, L20503, doi:10.1029/2004GL020919, 2004.
- Glagolev, M. V., Kleptsova, I. E., Filippov, I. V., Kazantsev, V. S., Machida, T., and Maksyutov, Sh. Sh.: Methane emissions from subtaiga mires of Western Siberia: The “standard model” Bc5, *Moscow University Soil Sci. Bull.*, 65, 86–93, 2010.
- Glagolev, M., Kleptsova, I., Filippov, I., Maksyutov, S., and Machida, T.: Regional methane emission from West Siberia mire landscapes, *Environ. Res. Lett.*, 6, 045214, doi:10.1088/1748-9326/6/4/045214, 2011.
- Glagolev, M. V., Sabrekov, A. F., Kleptsova, I. E., Filippov, I. V., Lapshina, E. D., Machida, T., and Maksyutov, Sh. Sh.: Methane Emission from Bogs in the Subtaiga of Western Siberia: The Development of Standard Model, *Eurasian Soil Sci.*, 45, 947–957, 2012.
- Glagolev, M. V., Filippov, I. V., Kleptsova, I. E., and Maksyutov, S. S.: Mathematical modeling in ecology/Proceedings of Third National Conference with International Participation (21–25 October 2013, Puschino, Russia), Puschino: Institute of Physical, Chemical and Biological Problems of Soils Science RAS, 75–76, 2013 (in Russian).
- Gorham, E.: Northern peatlands: role in the carbon cycle and probable responses to climate warming, *Ecol. Appl.*, 1, 182–195, 1991.
- Hauglustaine, D. A., Hourdin, F., Jourdain, L., Filiberti, M. A., Walters, S., Lamarque, J. F., and Holland, E. A.: Interactive chemistry in the Laboratoire de Météorologie Dynamique general circulation model: Description and background tropospheric chemistry evaluation, *J. Geophys. Res.-Atmos.*, 109, D04314, doi:10.1029/2003JD003957, 2004.
- Hodson, E. L., Poulter, B., Zimmermann, N. E., Prigent, C., and Kaplan, J. O.: The El Niño-Southern Oscillation and wetland methane interannual variability, *Geophys. Res. Lett.*, 38, L08810, doi:10.1029/2011GL046861, 2011.
- Hopcroft, P. O., Valdes, P. J., and Beerling, D. J.: Simulating idealized Dansgaard-Oeschger events and their potential impacts on the global methane cycle, *Quaternary Sci. Rev.*, 30, 3258–3268, 2011.
- Hydro1K: HYDRO1K: Website, available at: <https://lta.cr.usgs.gov/HYDRO1K> (last access: 1 April 2013), 2013.
- Intergovernmental Panel on Climate Change (IPCC): Climate Change 2013: The Physical Science Basis. Contribution of Working Group I to the Fifth Assessment Report of the Intergovernmental Panel on Climate Change, edited by: Stocker, T. F., Qin, D., Plattner, G.-K., Tignor, M., Allen, S. K., Boschung, J., Nauels, A., Xia, Y., Bex, V., and Midgley, P. M., Cambridge University Press, Cambridge, United Kingdom and New York, NY, USA, 1535 pp., doi:10.1017/CBO9781107415324, 2013.
- Ito, A. and Inatomi, M.: Use of a process-based model for assessing the methane budgets of global terrestrial ecosystems and evaluation of uncertainty, *Biogeosciences*, 9, 759–773, doi:10.5194/bg-9-759-2012, 2012.
- Kalnay, E., Kanamitsu, M., Kistler, R., Collins, W., Deaven, D., Gandin, L., Iredell, M., Saha, S., White, G., Woollen, J., Zhu, Y., Leetmaa, A., Reynolds, R., Chelliah, M., Ebisuzaki, W., Higgins, W., Janowiak, J., Mo, K. C., Ropelewski, C., Wang, J., Jenne, R., and Joseph, D.: The NCEP/NCAR 40-year reanalysis project, *B. Am. Meteorol. Soc.*, 77, 437–471, 1996.
- Kaplan, J. O.: Wetlands at the Last Glacial Maximum: Distribution and methane emissions, *Geophys. Res. Lett.*, 29, 1079, doi:10.1029/2001GL013366, 2002.
- Kaplan, J. O. and New, M.: Arctic climate change with a 2 degrees C global warming: Timing, climate patterns and vegetation change, *Clim. Change*, 79, 213–241, 2006.
- Kim, H.-K., Maksyutov, S., Glagolev, M. V., Machida, T., Patra, P. K., Sudo, K., and Inoue, G.: Evaluation of methane emissions from West Siberian wetlands based on inverse modeling, *Environ. Res. Lett.*, 6, 035201, doi:10.1088/1748-9326/6/3/035201, 2011.
- Kim, Y., Ueyama, M., Nakagawa, F., Tsunogai, U., Harazono, Y., and Tanaka, N.: Assessment of winter fluxes of CO<sub>2</sub> and CH<sub>4</sub> in boreal forest soils of central Alaska estimated by the profile method and the chamber method: a diagnosis of methane emis-

- sion and implications for the regional carbon budget, *Tellus B*, 59, 223–233, 2007.
- Kleinen, T., Brovkin, V., and Schuldt, R. J.: A dynamic model of wetland extent and peat accumulation: results for the Holocene, *Biogeosciences*, 9, 235–248, doi:10.5194/bg-9-235-2012, 2012.
- Koven, C. D., Ringeval, B., Friedlingstein, P., Ciais, P., Cadule, P., Khvorostyanov, D., Krinner, G., and Tarnocai, C.: Permafrost carbon-climate feedbacks accelerate global warming, *P. Natl. Acad. Sci. USA*, 108, 14769–14774, 2011.
- Kremenetski, K. V., Velichko, A. A., Borisova, O. K., MacDonald, G. M., Smith, L. C., Frey, K. E., and Orlova, L. A.: Peatlands of the Western Siberian lowlands: current knowledge on zonation, carbon content and late Quaternary history, *Quaternary Sci. Rev.*, 22, 703–723, 2003.
- Lawrence, D. M. and Slater, A. G.: Incorporating organic soil into a global climate model, *Clim. Dynam.*, 30, 145–160, 2008.
- Lawrence, D. M. and Slater, A. G.: The contribution of snow condition trends to future ground climate, *Clim. Dynam.*, 34, 969–981, 2010.
- Lehner, B. and Döll, P.: Development and validation of a global database of lakes, reservoirs, and wetlands, *J. Hydrol.*, 296, 1–22, 2004.
- Liang, X., Lettenmaier, D. P., Wood, E. F., and Burges, S. J.: A simple hydrologically based model of land surface water and energy fluxes for GSMs, *J. Geophys. Res.-Atmos.*, 99, 14415–14428, 1994.
- Liu, M., Tian, H., Yang, Q., Yang, J., Song, X., Lohrenz, S. E., and Cai, W.: Long-term trends in evapotranspiration and runoff over the drainage basins of the Gulf of Mexico during 1901–2008, *Water Resour. Res.*, 49, 1988–2012, 2013.
- Lupascu, M., Wadham, J. L., Hornibrook, E. R. C., and Pancost, R. D.: Temperature sensitivity of methane production in the permafrost active layer at Stordalen, Sweden: a comparison with non-permafrost northern wetlands, *Arct. Antarct. Alp. Res.*, 44, 469–482, 2012.
- Maksyutov, S., Patra, P. K., Onishi, R., Saeki, T., and Nakazawa, T. NIES/FRCGC global atmospheric tracer transport model: description, validation, and surface sources and sinks inversion, *Earth Simulator*, 9, 3–18, 2008.
- Markov, V. S. (Ed.): *Karta torfyanykh mestorozhdeniy Zapadno-Sibierskoi ravniny* (Map of peat deposits of West Siberian lowland), scale 1 : 1000 000, *Geol'trofrazvedka*, Moscow, 1971.
- Matthews, E. and Fung, I.: Methane emissions from natural wetlands: Global distribution, area, and environmental characteristics of sources, *Global Biogeochem. Cy.*, 1, 61–86, 1987.
- Matukhin, R. G. and Danilov, V. P. (Eds.): *Karta torfyanykh mestorozhdeniy Zapadnoi Sibiri* (Map of peat deposits of West Siberia), *Ministerstvo Prirodnikh resursov Rossiiskoi Federatsii, Sibirskii NII geologii, Geofiziki i Mineralnogo Syrja*, scale 1 : 1000 000, *Geol'trofrazvedka*, Moscow, 2000.
- Melton, J. R., Wania, R., Hodson, E., Poulter, B., Ringeval, B., Spahni, R., Bohn, T., Avis, C. A., Beerling, D. J., Chen, G., Eliseev, A. V., Denisov, S. N., Hopcroft, P. O., Lettenmaier, D. P., Riley, W. J., Singarayer, J. S., Subin, Z. M., Tian, H., Zurcher, S., Brovkin, V., van Bodegom, P. M., Kleinen, T., Yu, Z. C., and Kaplan, J. O.: Present state of global wetland extent and wetland methane modelling: Conclusions from a model intercomparison project (WETCHIMP), *Biogeosciences*, 10, 753–788, doi:10.5194/bg-10-753-2013, 2013.
- Mitsch, W. J. and J. G. Gosselink: *Wetlands*, Third Edition, John Wiley and Sons, Inc., New York, NY, USA, 2000.
- Mokhov, I. I., Eliseev, A. V., and Denisov, S. N.: Model diagnostics of variations in methane emissions by wetlands in the second half of the 20th century based on reanalysis data, *Doklady Earth Sci.*, 417, 1293–1297, 2007.
- Moore, T. R., de Young, A., Bubier, J. L., Humphreys, E. R., Lafleur, P. M., and Roulet, N. T.: A multi-year record of methane flux at the Mer Bleue bog, southern Canada, *Ecosystems*, 14, 646–657, 2011.
- NASA Land Processes Distributed Active Archive Center (LP DAAC), ASTER L1B, USGS/Earth Resources Observation and Science (EROS) Center, Sioux Falls, South Dakota, 2001.
- Naumov, E. M.: Soil map of the north-east of Eurasia, scale 1 : 2500 000, V. V. Dokuchaev Soil Inst., Moscow, 1993.
- Pace, M. L., Cole, J. J., Carpenter, S. R., Kitchell, J. F., Hodgson, J. R., Van de Bogert, M. C., Bade, D. L., Kirtzberg, E. S., and Bastviken, D.: Whole-lake carbon-13 additions reveal terrestrial support of aquatic food webs, *Nature*, 427, 240–243, 2004.
- Pan, S., Tian, H., Dangal, S. R. S., Zhang, C., Yang, J., Tao, B., Ouyang, Z., Wang, X., Lu, C., Ren, W., Banger, K., Yang, Q., Zhang, B., and Li, X.: Complex spatiotemporal responses of global terrestrial primary production to climate change and increasing atmospheric CO<sub>2</sub> in the 21st century, *PLoS One*, 9, e112810, doi:10.1371/journal.pone.0112810, 2014.
- Panikov, N. S. and Dedysh, S. N.: Cold season CH<sub>4</sub> and CO<sub>2</sub> emission from boreal peat bogs (West Siberia): Winter fluxes and thaw activation dynamics, *Global Biogeochem. Cy.*, 14, 1071–1080, 2000.
- Papa, F., Prigent, C., Aires, F., Jimenez, C., Rossow, W. B., and Matthews, E.: Interannual variability of surface water extent at the global scale, 1993–2004, *J. Geophys. Res.-Atmos.*, 115, D12111, doi:10.1029/2009JD012674, 2010.
- Peregon, A., Maksyutov, S., Kosykh, N. P., and Mironycheva-Tokareva, N. P.: Map-based inventory of wetland biomass and net primary production in western Siberia, *J. Geophys. Res.-Biogeosci.*, 113, G01007, doi:10.1029/2007JG000441, 2008.
- Peregon, A., Maksyutov, S., and Yamagata, Y.: An image-based inventory of the spatial structure of West Siberian wetlands, *Environ. Res. Lett.*, 4, 045014, doi:10.1088/1748-9326/4/4/045014, 2009.
- Petrescu, A. M. R., van Beek, L. P. H., van Huissteden, J., Prigent, C., Sachs, T., Corradi, C. A. R., Parmentier, F. J. W., and Dolman, A. J.: Modeling regional to global CH<sub>4</sub> emissions of boreal and arctic wetlands, *Global Biogeochem. Cy.*, 24, BG4009, doi:10.1029/2009GB003610, 2010.
- Prigent, C., Papa, F., Aires, F., Rossow, W. B., and Matthews, E.: Global inundation dynamics inferred from multiple satellite observations, 1993–2000, *J. Geophys. Res.-Atmos.*, 112, 305–317, 2007.
- Repo, M. E., Huttunen, J. T., Naumov, A. V., Chichulin, A. V., Lapshina, E. D., Bleuten, W., and Martikainen, J. T.: Release of CO<sub>2</sub> and CH<sub>4</sub> from small wetland lakes in western Siberia, *Tellus B*, 59, 788–796, 2007.
- Riley, W. J., Subin, Z. M., Lawrence, D. M., Swenson, S. C., Torn, M. S., Meng, L., Mahowald, N. M., and Hess, P.: Barriers to predicting changes in global terrestrial methane fluxes: analyses using CLM4Me, and methane biogeochemistry model integrated in

- CESM, *Biogeosciences*, 8, 1925–1953, doi:10.5194/gb-8-1925-2011, 2011.
- Ringeval, B., de Noblet-Ducoudré, N., Ciais, P., Bousquet, P., Prigent, C., Papa, F., and Rossow, W. B.: An attempt to quantify the impact of changes in wetland extent on methane emissions on the seasonal and interannual time scales, *Global Biogeochem. Cy.*, 24, GB2003, doi:10.1029/2008GB003354, 2010.
- Ringeval, B., Friedlingstein, P., Koven, C., Ciais, P., de Noblet-Ducoudré, N., Decharme, B., and Cadule, P.: Climate-CH<sub>4</sub> feedback from wetlands and its interaction with the climate-CO<sub>2</sub> feedback, *Biogeosciences*, 8, 2137–2157, doi:10.5194/bg-8-2137-2011, 2011.
- Rinne, J., Riutta, T., Pihlatie, M., Aurela, M., Haapanala, S., Tuovinen, J.-P., and Tuittila, E.-S.: Annual cycle of methane emission from a boreal fen measured by the eddy covariance technique, *Tellus B*, 59, 449–457, 2007.
- Rödenbeck, C., Gerbig, C., Trusilova, K., and Heimann, M.: A two-step scheme for high-resolution regional atmospheric trace gas inversions based on independent models, *Atmos. Chem. Phys.*, 9, 5331–5342, doi:10.5194/acp-9-5331-2009, 2009.
- Romanova, E. A., Bybina, R. T., Golitsyna, E. F., Ivanova, G. M., Usova, I. I., and Trushnikova, L. G.: Tipologicheskaya karta bolot Zapadno-Sibirskoi ravniny (Typological map of wetlands of West Siberian Lowland), scale 1 : 2500 000, GUGK, Moscow, 1977.
- Saarnio, S., Alm, J., Silvola, J., Lohila, A., Nykänen, H., and Martikainen, P. J.: Seasonal variation in CH<sub>4</sub> emissions and production and oxidation potentials at microsites of an oligotrophic pine fen, *Oecologia*, 110, 414–422, 1997.
- Sabrekov, A. F., Glagolev, M. V., Kleptsova, I. E., Machida, T., and Maksyutov, S. S.: Methane Emission from Bog Complexes of the West Siberian Taiga, *Eurasian Soil Sci.*, 46, 1182–1193, 2013.
- Sabrekov, A. F., Runkle, B. R. K., Glagolev, M. V., Kleptsova, I. E., and Maksyutov, S. S.: Seasonal variability as a source of uncertainty in the West Siberian regional CH<sub>4</sub> flux upscaling, *Environ. Res. Lett.*, 9, 045008, doi:10.1088/1748-9326/9/4/045008, 2014.
- Sasakawa, M., Shimoyama, K., Machida, T., Tsuda, N., Suto, H., Arshinov, M., Davydov, D., Fofonov, A., Krasnov, O., Saeki, T., Koyama, Y., and Maksyutov, S.: Continuous measurements of methane from a tower network over Siberia, *Tellus B*, 62, 403–416, 2010.
- Sasakawa, M., Ito, A., Machida, T., Tsuda, N., Niwa, Y., Davydov, D., Fofonov, A., and Arshinov, M.: Annual variation of CH<sub>4</sub> emissions from the middle Taiga in West Siberian Lowland (2005–2009): a case of high CH<sub>4</sub> flux and precipitation rate in the summer of 2007, *Tellus B*, 64, 17514, doi:10.3402/tellusb.v64i0.17514, 2012.
- Schaefer, K., Zhang, T., Bruhwiler, L., and Barrett, A. P.: Amount and timing of permafrost carbon release in response to climate warming, *Tellus B*, 63, 165–180, 2011.
- Schroeder, R., Rawlins, M. A., McDonald, K. C., Podest, E., Zimmermann, R., and Kueppers, M.: Satellite microwave remote sensing of North Eurasian inundation dynamics: development of coarse-resolution products and comparison with high-resolution synthetic aperture radar data, *Environ. Res. Lett.*, 5, 015003, doi:10.1088/1748-9326/5/1/015003, 2010.
- Schuldt, R. J., Brovkin, V., Kleinen, T., and Winderlich, J.: Modelling Holocene carbon accumulation and methane emissions of boreal wetlands – an Earth system model approach, *Biogeosciences*, 10, 1659–1674, doi:10.5194/bg-10-1659-2013, 2013.
- Schuur, E. A. G., Bockheim, J., Canadell, J. G., Euskirchen, E., Field, C. B., Goryachkin, S. V., Hagemann, S., Kuhry, P., LaFleur, P. M., Lee, H., Mazhitova, G., Nelson, F. E., Rinke, A., Romanovsky, V. E., Shiklomanov, N., Tarnocai, C., Venevsky, S., Vogel, J. G., and Zimov, S. A.: Vulnerability of permafrost carbon to climate change: Implications for the global carbon cycle, *Bioscience*, 58, 701–714, 2008.
- Serreze, M. C., Walsh, J. E., Chapin, F. S., Osterkamp, T., Dyurgerov, M., Romanovsky, V., Oechel, W. C., Morison, J., Zhang, T., and Barry, R. G.: Observational evidence of recent change in the northern high-latitude environment, *Clim. Change*, 46, 159–207, 2000.
- Sheng, Y., Smith, L. C., MacDonald, G. M., Kremenetski, K. V., Frey, K. E., Velichko, A. A., Lee, M., Beilman, D. W., and Dubinin, P.: A high-resolution GIS-based inventory of the west Siberian peat carbon pool, *Global Biogeochem. Cy.*, 18, GB3004, doi:10.1029/2003GB002190, 2004.
- Shimoyama, K., Hiyama, T., Fukushima, Y., and Inoue, G.: Seasonal and interannual variation in water vapor and heat fluxes in a West Siberian continental bog, *J. Geophys. Res.-Atmos.*, 108, 4648, doi:10.1029/2003JD003485, 2003.
- Sippel, S. J. and Hamilton, S. K.: Determination of inundation area in the Amazon River floodplain using the SMMR 37 GHz polarization difference, *Remote Sens. Environ.*, 76, 70–76, 1994.
- Smith, L. C., Sheng, Y., MacDonald, G. M., and Hinzman, L. D.: Disappearing arctic lakes, *Science*, 308, 1429–1429, 2005.
- Spahni, R., Wania, R., Neef, L., van Weele, M., Pison, I., Bousquet, P., Frankenberg, C., Foster, P. N., Joos, F., Prentice, I. C., and van Velthoven, P.: Constraining global methane emissions and uptake by ecosystems, *Biogeosciences*, 8, 1643–1665, doi:10.5194/bg-8-1643-2011, 2011.
- Spahni, R., Joos, F., Stocker, B. D., Steinacher, M., and Yu, Z. C.: Transient simulations of the carbon and nitrogen dynamics in northern peatlands: from the Last Glacial Maximum to the 21st century, *Clim. Past*, 9, 1287–1308, doi:10.5194/cp-9-1287-2013, 2013.
- Stocker, B. D., Roth, R., Joos, F., Spahni, R., Steinacher, M., Zährle, S., Bouwman, L., and Prentice, I. C.: Multiple greenhouse-gas feedbacks from the land biosphere under future climate change scenarios, *Nature Clim. Change*, 3, 666–672, 2013.
- Stocker, B. D., Spahni, R., and Joos, F.: DYP TOP: a cost-efficient TOPMODEL implementation to simulate sub-grid spatio-temporal dynamics of global wetlands and peatlands, *Geosci. Model Dev.*, 7, 3089–3110, doi:10.5194/gmd-7-3089-2014, 2014.
- Strack, M., Waddington, J. M., and Tuittila, E.-S.: Effect of water table drawdown on northern peatland methane dynamics: Implications for climate change, *Global Biogeochem. Cy.*, 18, GB4003, doi:10.1029/2003GB002209, 2004.
- Subin, Z. M., Milly, P. C., Sulman, B. N., Malyshev, S., and Shevliakova, E.: Resolving terrestrial ecosystem processes along a sub-grid topographic gradient for an earth-system model, *Hydrol. Earth Syst. Sci. Discuss.*, 11, 8443–8492, doi:10.5194/hessd-11-8443-2014, 2014.
- Tapley, B. D., Bettadpur, S., Ries, J. C., Thompson, P. F., and Watkins, M. M.: GRACE measurements of mass variability in the Earth system, *Science*, 305, 503–505, 2004.

- Tang, J. and Zhuang, Q.: Equifinality in parameterization of process-based biogeochemistry models: A significant uncertainty source to the estimation of regional carbon dynamics, *J. Geophys. Res.-Biogeosci.*, 113, G04010, doi:10.1029/2008JG000757, 2008.
- Tarnocai, C., Adams, G. D., Glooschenko, V., Glooschenko, W. A., Grondin, P., Hirvonen, H. E., Lynch-Stewart, P., Mills, G. F., Oswald, E. T., Pollett, F. C., Rubec, C. D. A., Wells, E. D., and Zoltai, S. C.: The Canadian wetland classification system, in: *Wetlands of Canada, Ecological Land Classification Series 24*, Environment Canada, Ottawa, Ontario, and Polyscience Publications, Montreal, Quebec, 413–427, 1988.
- Tarnocai, C., Canadell, J. G., Schuur, E. A. G., Kuhry, P., Mazhitova, G., and Zimov, S.: Soil organic carbon pools in the northern circumpolar permafrost region, *Global Biogeochem. Cy.*, 23, GB2023, doi:10.1029/2008GB003327, 2009.
- Tian, H., Xu, X., Liu, M., Ren, W., Zhang, C., and Lu, C.: Spatial and temporal patterns of CH<sub>4</sub> and N<sub>2</sub>O fluxes in terrestrial ecosystems of North America during 1979–2008: application of a global biogeochemistry model, *Biogeosciences*, 7, 2673–2694, doi:10.5194/bg-7-2673-2010, 2010.
- Tian, H., Melillo, J., Lu, C., Kicklighter, D., Liu, M., Ren, W., Xu, X., Chen, G., Zhang, C., Pan, S., Liu, J., and Running, S.: China's terrestrial carbon balance: contributions from multiple global change factors, *Global Biogeochem. Cy.*, 25, 222–240, 2011a.
- Tian, H., Xu, X., Lu, C., Liu, M., Ren, W., Chen, G., Melillo, J., and Liu, J.: Net exchanges of CO<sub>2</sub>, CH<sub>4</sub>, and N<sub>2</sub>O between China's terrestrial ecosystems and the atmosphere and their contributions of global climate warming, *J. Geophys. Res.-Biogeosci.*, 116, G02011, doi:10.1029/2010JG001393, 2011b.
- Tian, H., Lu, G., Chen, G., Tao, S., Pan, S., Del Grosso, S. J., Xu, X., Bruhwiler, L., Wofsy, S. C., Kort, E. A., and Prior, S. A.: Contemporary and projected biogenic fluxes of methane and nitrous oxide in terrestrial ecosystems of North America, *Front. Ecol. Environ.*, 10, 528–536, 2012.
- Trusilova, K., Rödenbeck, C., Gerbig, C., and Heimann, M.: Technical Note: A new coupled system for global-to-regional down-scaling of CO<sub>2</sub> concentration estimation, *Atmos. Chem. Phys.*, 10, 3205–3213, doi:10.5194/acp-10-3205-2010, 2010.
- Ulmishek, G. F.: *Petroleum geology and resources of the West Siberian Basin, Russia*, US Department of the Interior, US Geological Survey, Washington, DC, 2003.
- Umezawa, T., Machida, T., Aoki, S., and Nakazawa, T.: Contributions of natural and anthropogenic sources to atmospheric methane variations over western Siberia estimated from its carbon and hydrogen isotopes, *Global Biogeochem. Cy.*, 26, GB4009, doi:10.1029/2011GB004232, 2012.
- van Huissteden, J., Petrescu, A. M. R., Hendriks, D. M. D., and Rebel, K. T.: Sensitivity analysis of a wetland methane emission model based on temperate and arctic wetland sites, *Biogeosciences*, 6, 3035–3051, doi:10.5194/bg-6-3035-2009, 2009.
- Viovy, N. and Ciais, P.: CRUNCEP data set for 1901–2008, Tech. Rep. Version 4, Laboratoire des Sciences du Climat et de l'Environnement, available at: <http://dods.extra.cea.fr/data/p529viov/cruncep/>, last access: 1 September 2011.
- Walter, B. P. and Heimann, M.: A process-based, climate-sensitive model to derive methane emissions from natural wetlands: Application to five wetland sites, sensitivity to model parameters, and climate, *Global Biogeochem. Cy.*, 14, 745–765, 2000.
- Walter, K. M., Zimov, S. A., Chanton, J. P., Verbyla, D., and Chapin, F. S.: Methane bubbling from Siberian thaw lakes as a positive feedback to climate warming, *Nature*, 443, 71–75, 2006.
- Wania, R., Ross, I., and Prentice, I. C.: Integrating peatlands and permafrost into a dynamic global vegetation model: 1. Evaluation and sensitivity of physical land surface processes, *Global Biogeochem. Cy.*, 23, GB3014, doi:10.1029/2008GB003412, 2009a.
- Wania, R., Ross, I., and Prentice, I. C.: Integrating peatlands and permafrost into a dynamic global vegetation model: 2. Evaluation and sensitivity of vegetation and carbon cycle processes, *Global Biogeochem. Cy.*, 23, GB3015, doi:10.1029/2008GB003413, 2009b.
- Wania, R., Ross, I., and Prentice, I. C.: Implementation and evaluation of a new methane model within a dynamic global vegetation model: LPJ-WHYMe v1.3.1, *Geosci. Model. Dev.*, 3, 565–584, doi:10.5194/gmd-3-565-2010, 2010.
- Wania, W., Melton, J. R., Hodson, E. L., Poulter, B., Ringeval, B., Spahni, R., Bohn, T., Avis, C. A., Chen, G., Eliseev, A. V., Hopcroft, P. O., Riley, W. J., Subin, Z. M., Tian, H., van Bodegom, P. M., Kleinen, T., Yu, Z. C., Sinarayer, J. S., Zürcher, S., Lettenmaier, D. P., Beerling, D. J., Denisov, S. N., Prigent, C., Papa, F., and Kaplan, J. O.: Present state of global wetland extent and wetland methane modelling: methodology of a model inter-comparison project (WETCHIMP), *Geosci. Model Dev.*, 6, 617–641, doi:10.5194/gmd-6-617-2013, 2013.
- WETCHIMP-WSL: [http://arve.unil.ch/pub/wetchimp/wetchimp\\_wsl](http://arve.unil.ch/pub/wetchimp/wetchimp_wsl), last access: 21 January, 2015.
- Winderlich, J.: Setup of a CO<sub>2</sub> and CH<sub>4</sub> measurement system in Central Siberia and modeling of its results, Technical Reports 26, Max-Planck-Institut für Biogeochemie, Jena, p. 120, 2012.
- Winderlich, J., Chen, H., Gerbig, C., Seifert, T., Kolle, O., Lavrič, J. V., Kaiser, C., Höfer, A., and Heimann, M.: Continuous low-maintenance CO<sub>2</sub> / CH<sub>4</sub> / H<sub>2</sub>O measurements at the Zotino Tall Tower Observatory (ZOTTO) in Central Siberia, *Atmos. Meas. Tech.*, 3, 1113–1128, doi:10.5194/amt-3-1113-2010, 2010.
- Zhang, T.: Influence of the seasonal snow cover on the ground thermal regime: an overview, *Rev. Geophys.*, 43, RG4002, doi:10.1029/2004RG000157, 2005.
- Zhu, X., Zhuang, Q., Lu, X., and Song, L.: Spatial scale-dependent land-atmosphere methane exchanges in the northern high latitudes from 1993 to 2004, *Biogeosciences*, 11, 1693–1704, doi:10.5194/bg-11-1693-2014, 2014.
- Zhuang, Q., Melillo, J. M., Kicklighter, D. W., Prinn, R. G., McGuire, A. D., Steudler, P. A., Felzer, B. S., and Hu, S.: Methane fluxes between terrestrial ecosystems and the atmosphere at northern high latitudes during the past century: A retrospective analysis with a process-based biogeochemistry model, *Global Biogeochem. Cy.*, 18, GB3010, doi:10.1029/2004GB002239, 2004.
- Zürcher, S., Spahni, R., Joos, F., Steinacher, M., and Fischer, H.: Impact of an abrupt cooling event on interglacial methane emissions in northern peatlands, *Biogeosciences*, 10, 1963–1981, doi:10.5194/bg-10-1963-2013, 2013.